Nano Research

Open Access

Review Article

Recent research progress in the integration of Raman spectroscopy with machine learning algorithms for disease diagnosis

Zefeng Zheng[1,2,§], Ying Cui[3,§], Boyou Zhang[4,§], Yang Li[1,2], Yongjie Liu[1,2], Jiaying Ye[5], Feng Yuan[6], Khek-yu HO[7] ✉, Jing Liu[1,2] ✉, and Lijia Wang[1,2] ✉

[1] *Children's Hospital, Zhejiang University School of Medicine, National Clinical Research Center for Child Health, National Children's Regional Medical Center, Hangzhou 310052, China*
[2] *Zhejiang Key Laboratory of Neonatal Diseases, Hangzhou 310052, China*
[3] *Key Laboratory of Functional Metal-Organic Compounds of Hunan Province, College of Chemistry and Materials Science, Hengyang Normal University, Hengyang 421001, China*
[4] *Department of Thoracic Surgery, Sir Run Run Shaw Hospital, Zhejiang University School of Medicine, Hangzhou 310052, China*
[5] *Liberal arts and sciences, University of Washington, Seattle, WA 98195, USA*
[6] *Department of Thoracic Surgery, Zhejiang Hospital, Hangzhou 310013, China*
[7] *Department of Medicine, National University of Singapore, Singapore 119077, Singapore*
[§] *Zefeng Zheng, Ying Cui, and Boyou Zhang contributed equally to this work.*

Cite this article: *Nano Research*, **2025**, *18*, 94907834. https://doi.org/10.26599/NR.2025.94907834

ABSTRACT: Disease diagnosis involves multiple complex factors, and Raman spectroscopy has great potential to aid in diagnosis. While traditional Raman spectroscopy technology offers abundant chemical information, it may face challenges in highly complex pattern recognition tasks. As an emerging technology, artificial intelligence enhances multi-dimensional data processing via its learning and feature extraction capabilities while simulating human intelligence to achieve self-learning, self-optimization, self-adaptation, and autonomous decision-making. This enables automation, intelligent operation, and high-efficiency tasks. This review expounds on recent progress (over the past several years) in disease detection via the integration of Raman spectroscopy and machine learning, particularly in diagnosing cancers (e.g., gastrointestinal, urogenital, respiratory, and nervous systems) along with viral, bacterial, and fungal infections. This review demonstrates cross-disciplinary cooperation among fields like Raman spectroscopy, nanotechnology, and artificial intelligence, which has promoted biomedical detection technology. These technological advancements have not only refined diagnostic accuracy but also opened new avenues for research.

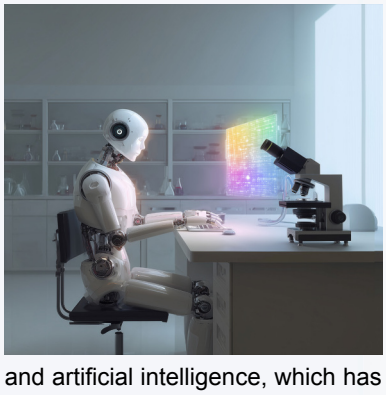

KEYWORDS: Raman spectroscopy, artificial intelligence, machine learning, disease diagnosis

1 Introduction

Raman spectroscopy is an analytical approach that captures molecular vibration spectra and provides detailed molecular information based on the Raman scattering effect, with predominant use in chemical analysis, mineral characterization, biomedical research and other fields [1]. In biomedicine, Raman spectroscopy represents a powerful tool that can be used to characterize biological systems, offering many advantages such as fast analysis, sensitivity, non-destructiveness, non-invasiveness, facile sample preparation, and good reproducibility [2–5]. Although Raman spectroscopy has been widely used in biomedical research, its clinical application remains limited due to the significant gap between basic research and practical diagnostic needs [6, 7]. Thus, it is still absent from routine hospital diagnoses.

Due to the complexity of clinical Raman spectral data, multivariate analysis is essential to comprehensively assess the significance of differences between groups [8]. At this point, it's not feasible to meet the demands for a complete assessment of all data and a comparison of group disparities solely through manual efforts, necessitating the support of artificial intelligence to avoid subjective biases [9]. As a pivotal branch of artificial intelligence, machine learning (ML) has made remarkable progress, which

Received: April 16, 2025; **Revised:** July 22, 2025
Accepted: July 23, 2025

✉Address correspondence to Khek-yu HO, khek_yu_ho@nuhs.edu.sg; Jing Liu, jing_liu@fudan.edu.cn; Lijia Wang, wanglijia@zju.edu.cn

facilitating the expansion of stoichiometry while enabling more accurate, automated, and faster analysis [10, 11]. Therefore, machine learning is expected to facilitate the transition of Raman spectroscopy from laboratory research to clinical practice [6, 12]. First, machine learning enables efficient processing of large-scale sample data. Besides, machine learning can extract valuable information from low signal-to-noise ratio data. In addition, machine learning identifies subtle changes in complex hidden features in large-sample data through data visualization, mining the correlation between signals and biological events. Last but not least, machine learning reduces the reliance on human expert interpretation.

Machine learning algorithms, including K-nearest Neighbor, support vector machine (SVM), and naive Bayes, have been integrated with Raman spectroscopy as ongoing methodological innovations to enhance analytical performance [13]. Research by Josef Brandt et al. introduced innovative methods in the treatment of spectra [14]. They proposed a deep learning method called auto-coded neural networks to remove instrumental noise and unwanted spectral artifacts in Fourier transform infrared and Raman spectroscopy, enabling efficient and automated spectrum acquisition. In addition, innovations in machine learning models have been achieved. Siheng Luo et al. established a new framework based on machine learning algorithms that integrated visual random forests (RF), feature amplifiers and data augmentation techniques for target trace analysis, demonstrating strong reliability and sensitivity [15].

This review comprehensively examines recent progress made in disease detection through the integration of Raman spectroscopy and ML, particularly in the diagnosis of brain, cervical, thyroid, breast, and liver cancer, as well as viral, bacterial, and fungal infections. With the help of ML algorithms, Raman spectroscopy is expected to become a novel approach suitable for medical diagnosis, with strong application potential and broad development prospects.

2 Pathogen infection diagnosis

Pathogens (viruses, bacteria, and fungi) are major causes of human infections, varying in pathogenicity and harm. Many are highly transmissible, leading to infectious diseases that have historically caused devastating outbreaks, significantly impacting global health, economies, and societies [16]. Therefore, rapid and accurate identification of pathogens that cause infections is key to controlling the spread of infections, developing effective preventive measures, and efficiently delivering patient treatment plans. Raman spectroscopy provides detailed information on the chemical composition of pathogens, combining rapid analysis with culture-free operation, and does not require the use of harmful dyes or markers. With the help of machine learning algorithms, Raman spectroscopy is expected to emerge as a major tool for the diagnosis of viral, bacterial, and fungal infections [17–19].

2.1 Virus infection diagnosis

Viruses are nanoscale microorganisms with a simple structural organization. Most viruses are contagious, and severe outbreaks can occur when highly pathogenic viruses spread. The outbreak of coronavirus disease 2019 (COVID-19) has highlighted the importance of rapid and sensitive virus detection for disease prevention and control. Accordingly, the application of Raman spectroscopy combined with machine learning in virus detection has attracted significant interest.

Yang et al. developed a label-free viral diagnostic platform using a SiO_2-coated silver nanorod surface enhanced Raman scattering (SERS) substrate combined with machine learning (SVM, RF, CNN, KNN, and Linear Discriminant Analysis (LDA)) to detect 13 respiratory viruses (including SARS-CoV-2) in saliva with > 99% accuracy [20]. The training process utilized stratified data splitting (90:10 for classification, 70:30 for regression) with hyperparameter optimization via 10-fold cross-validation (tuning regularization E, kernel coefficient γ, and tolerance ε). Feature selection was intrinsically guided by Raman peak significance, where baseline-corrected spectra (using Gaussian-Lorentzian function fitting) were normalized at 320 cm^{-1} and by mean intensity, with key discriminative wavenumbers (e.g., SARS-CoV-2's 735 cm^{-1} peak) identified through SVM feature importance analysis.

Performance was evaluated using accuracy (> 99%), precision/recall (macro/micro), F1-scores, area under curve (AUC, > 99% for all 16 classes), and for regression, mean absolute error and R^2 (0.80–0.99). Performance validation confirmed the models' physicochemical basis through feature importance mapping and virus-specific peak pattern recognition, though regression accuracy declined for untrained concentrations. This integrated SERS-ML approach enabled both rapid viral identification and quantitative analysis while maintaining clinical-grade accuracy.

For SARS-CoV-2 detection, different bases have been used to refine SERS spectral detection sensitivity [21, 22]. These studies utilized shell-isolated nanoparticle-enhanced Raman spectroscopy as the Raman-active substrate. The application of shell-isolated nanoparticle-enhanced Raman spectroscopy in rapid biomarker detection represents a new significant advancement in optical analysis and detection. It has been established that SiO_2 coating can effectively prevent the oxidation of silver nanorods. Moreover, compared to the precious metal Au, Ag is cheaper and demonstrates stronger Raman enhancement performance. However, it remains to be further investigated whether the virus can access the designated hotspot regions during the detection process when utilizing the SiO_2-coated silver nanorods array substrate, thereby facilitating SERS detection and recognition. It is widely thought that a greater proportion of test samples will not merely adhere to the surface of the SiO_2-coated silver nanorods array substrate due to surface tension effects, but penetrate into the intermediate and lower strata through aggregation or capture mechanisms. This would enhance signal intensity and enable more comprehensive analysis and identification of additional spectral features.

The clinical diagnosis of SARS-CoV-2 infection relies on throat or nasopharyngeal swab sampling. In recent years, Raman spectroscopy combined with machine learning has been applied to SARS-CoV-2 detection in throat or nasopharyngeal swab samples. Jinglin Huang et al. used SERS to detect SARS-CoV-2 antigen in throat swabs or sputum samples from 30 COVID-19 patients, establishing a Raman database based on the spike protein of SARS-CoV-2, and a residual neural network (ResNet)-based deep learning model pretrained on the database to predict SARS-CoV-2 antigen, yielding a recognition accuracy of 87.7% [23].

Their ResNet (comprising initial convolution → batch normalization → ReLU → max pooling → 5 blocks [1 convolution + 2 identity blocks] → average pooling → fully connected layer) achieved 87.7% accuracy (83.3% sensitivity, 92.5% specificity) with AUC = 0.846. The model was trained on a semi-synthetic dataset (187,500 spectra: 93,750 negative from healthy controls and 93,750

positive generated by superimposing modulated S-protein spectra) with 95:5 train-test split. Preprocessing included cosmic noise removal (43-point window), normalization, 5-point convolution filtering, and SNIP background correction, using raw spectra (618–1689 cm^{-1}) without feature selection. The approach demonstrated biological validity through key S-protein peaks (853, 1003, and 1586 cm^{-1}), DFT-calculated S1 subunit spectra, and differentiation via virus-specific amide I/III bands, though model interpretability remained limited to indirect biochemical validation rather than explicit explainability methods.

In a similar vein, another study led by Yanjun Yang et al. developed a SERS sensor based on a silver nanorod array substrate immobilized with DNA probes to specifically capture SARS-CoV-2 RNA (Fig. 1(a)) [24]. A recurrent neural network (RNN)-based deep learning model was developed to classify 40 positive and 120 negative specimens with an overall accuracy of 98.9%. For the blind test of 72 specimens, the RNN model gave a 97.2% accuracy prediction for positive specimens and a 100% accuracy for negative specimens.

This study employs multiple ML/DL models—including SVM, RF, Backpropagation Neural Network (BP), CNN, and RNN-with the RNN (featuring three LSTM layers: 1200, 600, and 300 units + dense layer) achieving optimal performance. Models were trained on SERS spectra from DNA-functionalized AgNR substrates using a 7:3 stratified split (1758 positive/1652 negative spectra for training; 754 positive/708 negative for testing). Adam optimization (learning rates 0.003–0.09) with L2 regularization and 170-epoch training minimized cross-entropy loss. Feature selection used occlusion-based importance mapping, identifying key peaks (e.g., 1329 cm^{-1} contribution = 0.993, 794 cm^{-1} = 0.644) that linearly correlated with intensity. Evaluation metrics included accuracy (RNN: 98.9% test, 97.2% blind positive, 100% negative), ROC/AUC (0.9892), and confusion matrices. Validation combined standard train-test splits and blind testing on 72 specimens using a γ-threshold strategy ($\gamma = n_+/(n_+ + n_-) > 0.7$ for positivity).

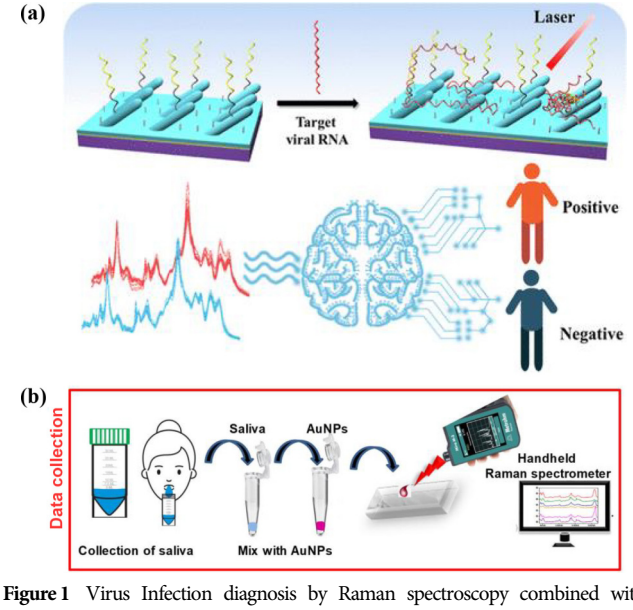

Figure 1 Virus Infection diagnosis by Raman spectroscopy combined with machine learning. (a) Silver nanorod array wells, substrate preparation, viral RNA interaction with the DNA probe on the Silver nanorod array substrate, and SERS spectra collection. Implementation of the deep learning model to differentiate positive or negative infection using SERS spectra. Reproduced with permission from Ref. [24], © American Chemical Society 2022. (b) Schematic representation for workflow employed for the proposed strategy aiming COVID-19 diagnostics using SERS and artificial intelligence (AI) with saliva as the sample of choice. Reproduced with permission from Ref. [25], © Elsevier B.V. 2022.

Conventional nasopharyngeal swabs are invasive and uncomfortable, making saliva an attractive alternative for SARS-CoV-2 detection. Varsha Karunakaran et al. employed a portable Raman spectrophotometer with colloidal Au nanoparticles to analyze saliva from healthy, infected, and recovered subjects (Fig. 1(b)) [25]. Their SVM classifier achieved 95% accuracy in detecting infections by combining surface-enhanced Raman scattering with machine learning, demonstrating saliva's potential for non-invasive COVID-19 diagnosis.

This study employs a SVM classifier with Radial Basis Function kernel for multi-class discrimination (healthy/COVID-19 infected/recovered) using label-free salivary SERS spectra. The model architecture leverages Kernel Principal Component Analysis (KPCA) with Radial Basis Function kernel for feature extraction/dimensionality reduction, reducing 1650 spectral data points (500–2150 cm^{-1}) to 2 principal components. Training used a 75:25 train-test split with 5-fold cross-validation to mitigate overfitting. Feature selection was automated via KPCA, prioritizing nonlinear spectral patterns without manual peak selection. Evaluation metrics included accuracy (95.38%), F1-scores (healthy: 94.73%, infected: 95.28%, recovered: 94%), and confusion matrices. Data processing involved: raw spectra preprocessing (cosmic ray/noise removal via Miracal software); 4th-degree polynomial background subtraction; Savitzky-Golay smoothing; ARPLS baseline correction ($\lambda = 10^6$); 400–2300 cm^{-1} normalization; Validation combined independent test sets (25%) and 5-fold CV. The limitations of this study included small cohort size (n = 18 patients) and dependency on thiocyanate variance (smoking confounder) affected F1-scores in multi-class tasks (recovered: 94%).

Currently, a portable handheld Raman spectrophotometer can be used for on-site analysis and detection, reducing sample contamination and improving detection accuracy. However, this approach faces limitations when detecting samples with low viral loads, where spectral differentiation becomes challenging, and the sampling process poses certain health risks to testing personnel. Whether there are safer and more effective ways to collect samples for testing is a further research direction.

Gas detection has emerged as a promising application for SERS technology, with recent advances including instrument modifications, microfluidic chips, and even everyday face masks. Researchers have developed mask-integrated SERS sensors using cost-effective Au-TiO_2 nanocomposites, which enhance aerosol enrichment and boost signal intensity by 47% compared to conventional Au substrates [26]. By combining SERS spectral analysis with machine learning autoencoders, this approach achieved over 98% accuracy in quantitatively detecting SARS-CoV-2 in aerosols across a concentration range of 10^1–10^4 pfu/mL, demonstrating the potential for practical respiratory virus monitoring.

This study employs an ablation-assisted autoencoder with a symmetric architecture (1069 input nodes → 256-node fully connected layer → 36-node layer → 2D latent space) followed by logistic regression for quantitative SARS-CoV-2 detection in respiratory aerosols. The model was trained on SERS spectra (600–1580 cm^{-1}, 1096-point vectors) of SARS-CoV-2 lysates (0, 10^1–10^4 pfu/mL) in artificial respiratory aerosols, with data

augmented through synthetic noise injection (±20% amplitude) and SMOTE oversampling (shrinkage = 1.8). Key to the approach was the targeted ablation of non-discriminant Raman peaks at 1532 and 1587 cm^{-1}-dentified via intensity ratio analysis as interfered by aerosol matrix components-hich enhanced classification accuracy by 7.6%. The autoencoder was optimized using a custom loss function (combining latent, intraclass, interclass, and centroid distance losses) over 40 epochs (batch size 32, learning rate 10^{-4}), forcing concentration-dependent diagonal clustering in the latent space. Validated on a separate test set (475 synthetic + 25 experimental spectra), the ablation-assisted model achieved > 98% accuracy across 10^{1}–10^{4} pfu/mL via logistic regression, with performance quantified by ROC curves (macro-averaged) and confusion matrices.

Besides, Raman spectroscopy combined with machine learning has been applied to the detection of influenza A and B viruses. The SERS spectra of both viruses were obtained in a buffer environment and analyzed with machine learning to distinguish the two viruses with an accuracy of 93% [27]. This study uses a linear SVM classifier to detect influenza A/B viruses in buffer using raw SERS spectra (1332 data points) without feature selection. Spectra were preprocessed via standardization and normalization. Training employed stratified 9:1 cross-validation, achieving 93% accuracy for differentiating influenza A, B, and buffer. Sensitivity reached 0.05 μg/mL with 84% accuracy.

These SERS-AI diagnostic platforms share key advantages including rapid (< 30 min), non-invasive detection using portable systems (e.g., saliva, breath aerosols), clinically relevant high sensitivity, and robust AI-driven decoding of subtle spectral features masked by biological noise. However, they face common limitations: small clinical cohorts and synthetic data reliance limit real-world generalizability; complex biofluid matrices cause interference requiring advanced preprocessing; poor model interpretability obscures biomarker validation; inconsistent data handling and regulatory gaps hinder standardization; and performance declines at ultralow concentrations (e.g., 84% accuracy at 0.05 μg/mL). Collectively, while promising for point-of-care deployment, clinical translation demands larger validation trials, protocol standardization, and rigorous biomarker correlation to overcome matrix interference and algorithmic opacity.

2.2 Bacterial infection diagnosis

Bacterial infections are among the ten most common causes of death worldwide, with acute infections often being serious or even fatal [28]. Rapid detection of bacterial species and analysis of drug resistance trends are essential for effective treatment. Traditional diagnostic methods, such as culture isolation, biochemical and serological tests, and immunoassay, are time-consuming, labor-intensive, and expensive to perform. In recent years, many studies have adopted Raman spectroscopy technology combined with mechanical learning to achieve rapid detection of bacterial species and identify drug resistance patterns [29].

2.2.1 Identification of bacterial species

Raman spectroscopy is an analytical technique based on molecular vibrational spectroscopy that can achieve rapid identification and quantitative analysis of bacteria by obtaining their Raman fingerprint characteristics. Bacterial detection is predominantly conducted via both label-free and labeled methods. By enhancing the substrate and directly binding to bacterial cells, or using SERS probes for targeted detection, its unique intrinsic fingerprint features can be quickly obtained for analysis and identification. Through this technology, multiple bacteria can be detected simultaneously, and even the evaluation of bacterial resistance can be achieved. However, some bacterial cells exhibit weak Raman signals and complex background signals, which lead to interference. Besides, minimal spectral differences prevail between species, emphasizing the need for more advanced data analysis methods to improve detection sensitivity and specificity.

Recent advances have demonstrated machine learning's potential for bacterial identification through Raman spectroscopy, offering a rapid alternative to traditional culture methods [30–32]. Chi-Sing Ho et al. developed a 26-layer one-dimensional (1D) ResNet-based convolutional neural network (CNN) that processes raw bacterial spectra (1332 data points) using strided convolutions to preserve peak locations, achieving 99.7% identification accuracy for 30 common pathogens with just 10 spectra per sample [33].

This research employs a 26-layer 1D CNN based on a ResNet architecture with residual connections to identify 30 bacterial pathogens and their antibiotic susceptibility directly from noisy Raman spectra. The model processes raw spectral data (1332 data points) without explicit feature selection, using strided convolutions instead of pooling layers to preserve precise peak locations. Training involves two key phases: pre-training on a large reference dataset (60,000 spectra from 30 isolates) followed by fine-tuning on clinical isolates using leave-one-patient-out cross-validation (LOOCV). Hyperparameters include the Adam optimizer (learning rate 0.001) and batch size 10.

Performance is evaluated through isolate-level accuracy (82.2% ± 0.3%), empiric treatment identification accuracy (97.0% ± 0.3%), and MRSA/MSSA differentiation (89.1% ± 0.1%, AUC = 0.953). Validated on 50 patient isolates, the model achieves 99.7% treatment identification accuracy with just 10 spectra per sample—significantly outperforming SVM (74.9%) and logistic regression (75.7%) baselines.

Critically, the CNN deciphers phenotypic spectral fingerprints imperceptible to conventional analysis: it distinguishes isogenic MRSA/MSSA strains (differing only in *mecA* gene expression) by detecting subtle cell-wall composition changes linked to methicillin resistance, while overcoming high intra-sample spectral variance and low signal-to-noise ratios (SNR ~4.1) that mask bacterial features in raw spectra. This demonstrates deep learning's capacity to extract clinically actionable insights from inherently weak, complex Raman data where traditional methods fail. Despite the higher cost of gold versus silver nanorods, this method achieves minute-scale diagnosis by detecting subtle phenotypic fingerprints (SNR ~ 4.1) for targeted therapy, warranting future development of cost-effective silver substrates.

One study employed Raman spectroscopy to detect Clostridium difficile toxins A and B in stool samples by spiking negative samples with varying toxin concentrations [34]. After preprocessing (background subtraction, cosmic ray removal, and normalization), multiple machine learning models (SVM with linear/radial kernels, RF, gradient boosting machine, and PCA-linear discriminant analysis) were trained on 70% of the full-spectrum data (no manual peak selection) and tested on a 30% holdout set. The models achieved moderate accuracy (64%–77%), with sensitivity (69%–90%) exceeding specificity (43%–78%), suggesting an ability to detect subtle spectral patterns associated with toxins despite stool matrix interference. Performance varied by model-GBM, PCA-

LDA, and SVM-linear excelled at different toxin concentrations—and improved with larger datasets (as shown by RF learning curves). While natural stool variability and limited initial data (360 spectra from 36 samples) constrained results, the study highlights RS-ML's potential for toxin detection, with deep learning and expanded datasets likely to enhance accuracy.

Another study achieved serotype-level strain prediction. Shuaishuai Yan et al collected single-cell Raman spectroscopy of 23 strains from 7 different bacteria genera, and applied a four-level classification model to identify serotypes of bacteria [35]. The accuracy of identification models at different levels was between 87.1% and 95.8%. The study uses a KPCA-DT model (Kernel PCA + Decision Tree) to classify food-borne pathogens from single-cell Raman spectra (SCRS). Raw spectra undergo preprocessing: cosmic spike removal, background subtraction, baseline correction, smoothing (23-point Savitzky–Golay filter), and normalization. KPCA with an Radial Basis Function kernel extracts nonlinear discriminative features from the complex spectral data, overcoming linear PCA's limitations. The Decision Tree (using entropy-based splitting) then classifies strains based on these features. For validation, 10-fold cross-validation splits 15,890 SCRS into training/validation (9 subsets) and testing (1 subset), repeated 10 times.

Performance is measured by accuracy, specificity, sensitivity, AUC-ROC, and confusion matrices. The single KPCA-DT model achieved 86.2% accuracy but showed misclassification for similar strains (e.g., *Salmonella*). A four-tier hierarchical model (Gram-type → genus → species → serotype) improved accuracy to 87.1%–95.8% across levels. The ML models rely directly on Raman features: KPCA-derived nonlinear features (e.g., peaks like 1002 cm^{-1} reflecting biochemical differences) enable the Decision Tree to map spectra to biological classifications. These features encode intrinsic cellular properties (e.g., Gram-positive/negative cell wall differences), proving critical for fine-grained classification. PCA-SVM (73.5% accuracy) underperformed due to its linear feature extraction, confirming nonlinear KPCA features are essential for capturing subtle spectral variations. This synergy enables efficient, portable pathogen detection

The above findings demonstrate the potential of Raman spectroscopy combined with machine learning algorithms in accurately identifying and classifying bacterial infections at both the toxin and serotype levels. The heterogeneous accuracy rates suggest that while these methods are promising, there is still room for improvement in model optimization and data preprocessing techniques. Future research could focus on enhancing the sensitivity and specificity of these models by incorporating larger and more diverse datasets. Besides, exploring the integration of other biomarkers or complementary detection methods might further boost diagnostic accuracy. The application of such advanced techniques in clinical settings could significantly aid in the rapid and precise identification of bacterial pathogens, thereby guiding more effective treatment strategies and improving patient outcomes.

In a study that included gold nanorods in samples, Fareeha Safir et al. invented an acoustic bioprinter that can divide a sample into millions of tiny droplets, each containing just a few cells [13]. Solutions containing Staphylococcus epidermidis, Escherichia coli and blood were divided into small droplets containing only a few cells each, mixed with gold nanorods to enhance signal strength. Then the SERS spectrum was collected to trianed the machine learning model, and the accuracy of the classification of pure cell samples was greater than 99%, and the classification of mixed cell samples was greater than 87%.

It is now understood that samples are adsorbed on a solid substrate with a metal nanostructure or in a colloidal suspension of gold or silver nanoparticles [36]. SERS technology offers comprehensive information, achieves single-molecule sensitivity, and enables rapid, non-destructive analysis of trace and ultra-trace samples. This innovative approach not only significantly improves the efficiency of bacterial detection but also reduces the time required for diagnosis. The use of acoustic bioprinting technology allows precise control over the size and distribution of the droplets, which is crucial for the accurate identification of bacteria. The integration of AI-assisted Raman spectroscopy has further enhanced the specificity and sensitivity of the detection process, making it possible to distinguish between different bacterial species and strains based on their unique spectral signatures. The study's findings suggest that this method could be a game-changer in clinical settings, where rapid and accurate identification of pathogens is essential for effective treatment. The high-throughput nature of the technique facilitates rapid screening of large numbers of samples, potentially leading to faster diagnosis and better patient outcomes. Moreover, bacterial detection in blood samples could be beneficial in cases of sepsis, where early detection and identification of causative organisms are critical for patient survival.

By combining SERS and machine learning, Eojin Rho et al. collected the Raman signals of bacteria in various media, and realized the classification without the need for bacterial separation procedures [28]. In this study, the bacteria Escherichia coli and Staphylococcus epidermidis were inoculated into five different liquid media, after which the samples were dropped onto a silver-based SERS substrate and dried. After acquisition of the SERS spectra, machine learning was used to identify the signals of the medium and the bacteria, yielding a classification accuracy of 98%. Robert Hunter et al. designed an optical flow Raman detection platform that combines a microfluidic-driven hollow-core photonic crystal fiber with silver nanoparticles [37]. After capturing the Raman spectra of three different bacteria to establish the dataset, the count was optimized by machine learning, with a detection limit of 4 CFU/mL. Furkan Sahin et al synthesized an antibacterial Ag-Cuxo nanostructured plasmonic surface on paper substrate, which improved surface-enhanced Raman scattering activity (Fig. 2(a)) [38]. Using substrate-enhanced detection, the SERS spectra of five different bacteria were collected and combined with machine learning to achieve automated identification of bacteria with an accuracy of more than 96%.

This study demonstrates the potential of SERS combined with machine learning for rapid and accurate identification of bacterial species. This method could significantly enhance the efficiency of clinical diagnostics and reduce the time required for pathogen identification. Indeed, the ability to circumvent traditional bacterial culture and separation steps is beneficial in urgent cases where immediate identification is crucial. Furthermore, the high accuracy achieved in this study indicates that this approach could serve as a promising alternative to conventional microbiological methods, which are often time-consuming and labor-intensive. These findings pave the way for further research into the development of portable and user-friendly SERS-based diagnostic tools that could be utilized in a variety of settings, ranging from hospitals to remote areas with limited access to advanced laboratory facilities. In

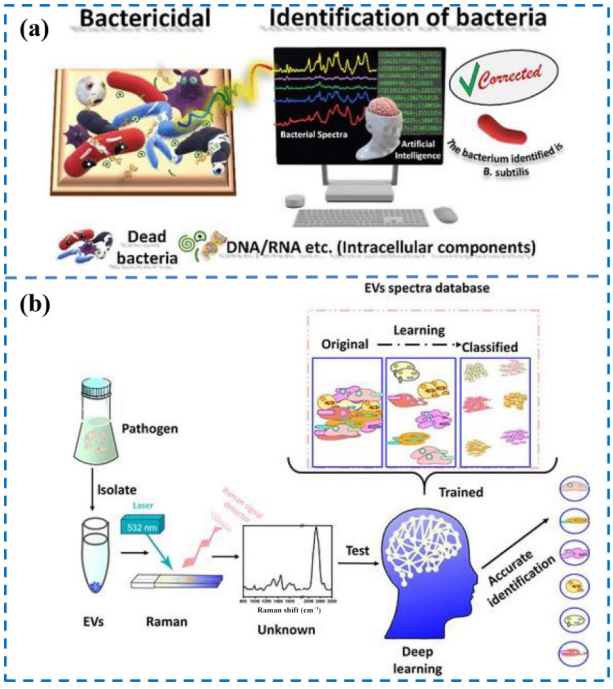

Figure 2 Bacterial infection diagnosis by Raman spectroscopy combined with machine learning. (a) Disintegration of bacteria on the Ag-Cu_xO nanostructures, and detection and identification of bacteria through the collected SERS spectra and classification using machine learning. Reproduced with permission from Ref. [38], © Sahin, F. et al. 2023. (b) A new deep learning model enabled Raman spectroscopic identification of pathogen-derived extracellular vesicles. Reproduced with permission from Ref. [44], © American Chemical Society 2022.

addition, the sensitivity of Raman spectroscopy is very high, making it susceptible to small fluctuations that may produce erroneous results. Besides, the spectrum of clinical samples is complex and highly heterogeneous, requiring robust methods for classification and analysis. Therefore, Raman spectroscopy technology still needs to be compared in real-time with databases during clinical application to provide accurate diagnostic results, which puts higher demands on the real-time processing ability and accuracy of the system.

2.2.2 *Bacterial resistance detection*

In addition to identifying bacterial species, Raman spectroscopy can also be applied to the detection of bacterial antibiotic resistance [39–41]. Xiaofei Yi et al. developed a rapid Raman-assisted antibiotic susceptibility test combining single-cell spectroscopy with machine learning [42]. Their approach integrated Gram-staining classification via Raman spectra, two-step antibiotic inhibition, heavy water labeling, and large-scale double-blind validation.

This study employed a LDA model to classify bacterial Gram-staining (GS) types using SCRS. The model was trained on a database of 8000 SCRS from four Gram-positive (GP) and four Gram-negative (GN) strains, with Principal Component Analysis (PCA) first reducing spectral dimensionality to highlight key features like C-H and C-D bands. These features were then used by LDA to distinguish GP from GN bacteria with high sensitivity (98.8% for GP, 94.3% for GN at the single-cell level) and accuracy (100% when > 90% of cells agreed). Validation on six independent clinical isolates confirmed robustness, even for species like Enterococcus faecium not in the training set. The Raman spectra, particularly metabolic markers such as deuterium incorporation (2040–2300 cm^{-1}), directly informed the model's decisions, linking biochemical activity to classification. Performance was assessed via agreement with conventional methods (87.7% for urine samples, 88% overall for antibiotic susceptibility), though cross-validation details were omitted. The pipeline involved SCRS acquisition, PCA-based feature extraction, and LDA classification, ensuring rapid, reliable GS prediction without culturing delays.

William John Thrift et al. developed a SERS-based sensor platform that rapidly detects antibiotic responses in Pseudomonas aeruginosa and Escherichia coli using a variational autoencoder (VAE) for spectral analysis, achieving > 99% accuracy in distinguishing treated from untreated cells [43]. The VAE compresses SERS spectra into a low-dimensional latent space capturing metabolic response patterns, including nucleotide degradation markers (1100–200 cm^{-1}) and deuterium incorporation (2040–2300 cm^{-1}). Subsequent deep neural networks and SVMs trained on these features classified bacterial responses within 10 min of antibiotic exposure, even at sub-MIC doses (0.1 μg/mL), while Bayesian Gaussian mixture models achieved 99.3% clustering accuracy.

The system employs data-informed transfer learning, using metabolite mixtures to enhance the VAE's feature representation and reduce labeled data requirements. Validated through 10-fold cross-validation (98%–99% accuracy), this approach correlates spectral biomarkers (e.g., aromatic metabolite vibrations) with phenotypic resistance, enabling culture-free antimicrobial susceptibility testing in minutes. This breakthrough transforms SERS into a rapid AST tool by decoding metabolic fingerprints through machine learning, significantly accelerating therapeutic decision-making while supporting personalized medicine and global antibiotic resistance efforts.

One article focused on the use of exosomes to identify bacterial drug resistance (Fig. 2(b)) [44]. Here, Qin et al. developed a novel attention-based neural network (aNN) for identifying bacterial drug resistance through label-free Raman spectroscopy of extracellular vesicles (EVs) from six pathogens (*Escherichia coli*, *Pseudomonas aeruginosa*, *Curtobacterium joostei*, *Salmonella enterica*, *Staphylococcus aureus*, and *Enterococcus faecalis*).

The aNN architecture combines convolutional layers with dual attention mechanisms that simultaneously analyze spectral channels and specific wavenumbers, enabling detection of subtle but discriminative features like the 1130 cm^{-1} band for *C. joostei* and 1413 cm^{-1} for *E. coli*. Trained on 4335 Raman spectra using weighted cross-entropy loss to address class imbalance, the model achieved 96.5% accuracy for Gram/species classification, 94% for strain identification (including drug-resistant vs. sensitive strains), and 87% for physiological state discrimination-outperforming conventional methods like SVM and PCA-LDA in both accuracy and computational efficiency. Integrated gradient analysis revealed the model's decision-making basis while simultaneously providing biological insights into EV biomolecular packaging differences from parent bacteria. The complete workflow encompassing label-free spectral acquisition, normalization, attention-based feature extraction, and gradient interpretation was validated on independent test sets, demonstrating robust performance for rapid, non-invasive antimicrobial resistance detection.

Raman spectroscopy offers comprehensive bacterial phenotypic information, but current spectral databases primarily rely on pure cultured isolates, leaving clinical sample data scarce. The technique generates complex spectral data from chemical mixtures,

necessitating AI-driven analysis rather than classical linear methods. While machine learning enables rapid, culture-free pathogen identification and antibiotic resistance profiling (achieving 80%–99% accuracy) by detecting subtle biochemical fingerprints, several challenges persist: (1) uneven substrate enhancement effects compromise SERS reproducibility; (2) high-dimensional data with limited samples risk overfitting or underfitting, despite dimensionality reduction techniques like PCA; (3) sensitivity to spectral noise and sample quality variations; (4) limited discriminative power for closely related strains; and (5) performance degradation in complex matrices (e.g., stool). Natural biological variability and operational expertise requirements further complicate clinical translation, though hierarchical classification and attention mechanisms help mitigate these issues.

Future advancements in Raman technology, nanostructured materials, computational methods, and standardized databases are poised to enable reliable automated clinical measurements, particularly for bacterial typing and resistance detection, pending expanded validation and optimization for real-world sample complexity.

2.3 Fungal infection detection

In recent years, the widespread use of hormones, immunosuppressants and broad-spectrum antibiotics in clinical practice has led to an increase in the number of immunocompromised people, resulting in a rise in the number of infections caused by fungi. Rapid and accurate identification of fungi has become the focus of etiological diagnosis.

In one project, María Gabriela Fernández-Manteca et al. collected and processed the Raman spectra of eleven species of the genus Candida [45]. Then trained several machine learning and deep learning algorithms using hyperparameter optimization techniques to find the best possible classifier for this spectral data, and found that a one-dimensional CNN could achieve above 80% overall accuracy for the eleven classes spectral dataset, with good generalization capabilities.

In a separate study, Natalie Arend et al. employed Raman spectroscopy to analyze neutrophils exposed to bacterial (*Staphylococcus aureus*, *Escherichia coli*) and fungal (*Candida albicans*) pathogens, compiling ~ 20,000 spectra [46]. This study combined Raman spectroscopy with machine learning to classify 11 *Candida* species using 3126 spectra. A 1D CNN was the best-performing model, featuring convolutional layers, dropout, and max-pooling to reduce overfitting. The spectra were preprocessed with normalization, smoothing, baseline correction, and feature selection (43 manually chosen spectral peaks and high-variance zones). The model was trained using 10-fold cross-validation and hyperparameter optimization, achieving 74% accuracy with additional metrics like F1-score (0.83 macro-average) and AUC. Data augmentation (mixing spectra, adding noise) and outlier removal (Isolation Forest) improved generalization. The 1D CNN worked well with raw spectra, while traditional models (e.g., SVM) relied more on selected features, showing that deep learning could better handle spectral variability. Y-randomization tests confirmed the model learned real patterns rather than noise.

Compared to bacteria, Raman spectroscopy combined with artificial intelligence for single-cell fungal analysis is still in its early stages, with only a few studies using a small number of standard strains or clinical isolates with limited sample coverage. Therefore, Raman spectroscopy combined with artificial intelligence still has a long way to go and is expected to play a greater role for the analysis of fungal single cells.

3 Diagnostics of cancer

According to the latest global cancer burden data released by the International Agency for Research on Cancer under the World Health Organization in 2020, China has become a veritable "cancer nation". The incidence of cancer is influenced by genes, diet, lifestyle habits, environmental exposure, immune function and other factors. While cancer has a high mortality rate, early diagnosis contributes to a good prognosis. Raman spectroscopy combined with machine learning holds great potential for rapid and high-precision diagnosis of cancer and other diseases (Fig. 3(a)) [47]. Studies have been conducted to diagnose cancer, such as destive system cancer, urogenital system cancer, respiratory system cancer and nervous system cancer [48–51].

Ningtao Cheng developed a SERS biosensor using ZnO nanocolumns modified with Au-Ag nanocomplexes to detect liver diseases through serum analysis [52]. This study presents a SERS-based biosensing platform for liver disease detection, integrating a ZnO/AgNP/AuNP nanoarray sensor with a custom CNN classifier. The CNN architecture comprises three sequential blocks of 1D convolutional layers (16 filters, 3 × 1 kernel), each followed by batch normalization, ReLU activation, and max pooling (stride = 2), culminating in a dropout layer (0.5) and softmax classification. The model was trained on 450 preprocessed SERS spectra

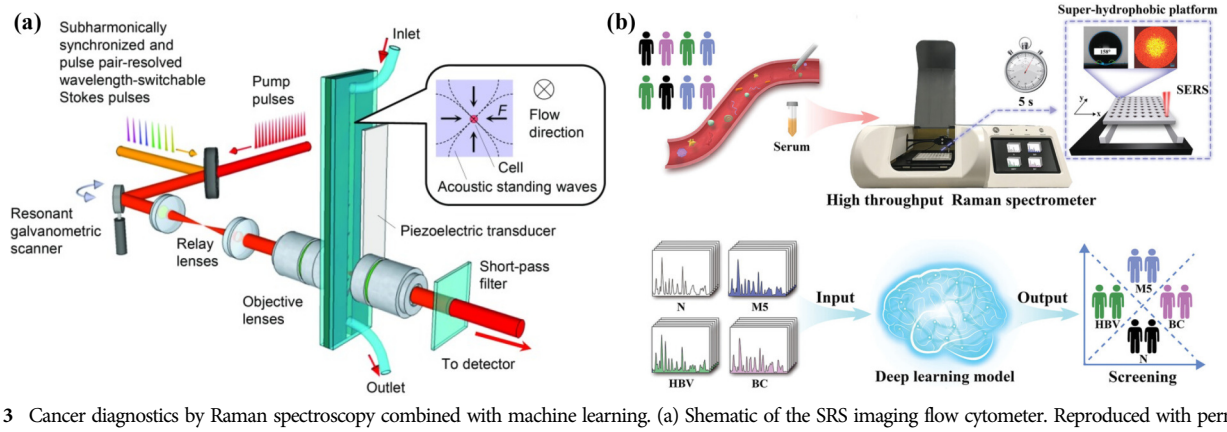

Figure 3 Cancer diagnostics by Raman spectroscopy combined with machine learning. (a) Shematic of the SRS imaging flow cytometer. Reproduced with permission from Ref. [53], © Suzuki, Y. et al. 2019. (b) Schematic of the high-throughput and super-hydrophobic SERS platform for bladder cancer, M5, hepatitis B virus, and N screening. Reproduced with permission from Ref. [57], © Wiley-VCH GmbH 2021.

(400–1800 cm^{-1}) from serum samples (normal/HCC/HB), using SGDM optimization (initial LR = 0.01, L2 = 0.001) with minibatches of 45 spectra, achieving 97.78% test accuracy. Spectral preprocessing included background subtraction, Savitzky–Golay smoothing, and min–max normalization, with data split into training (90%) and test sets (10%) via stratified sampling.

Validation employed 5-fold cross-validation (95.31% accuracy) and independent testing, demonstrating the CNN's ability to automatically extract discriminative features from subtle spectral patterns despite lacking obvious characteristic peaks. The model's hierarchical learning correlates molecular vibration patterns with disease states through progressively abstract representations, outperforming manual feature extraction methods.

The ZnO/AgNP/AuNP nanoarray provided high sensitivity (AEF = 1.02×10^7), while spectral preprocessing (background subtraction, Savitzky–Golay smoothing, and normalization) ensured data quality. Despite its success with limited samples (30 patients/class), future work should expand the dataset and adopt patient-wise splitting to improve generalizability for diverse populations. This approach showcases the potential of combined SERS-CNN platforms for non-invasive, early disease detection.

Flow cytometry, a laser-based technique for analyzing cell or particle properties, is limited by its reliance on fluorescent labeling. Yuta Suzuki et al. developed a label-free chemical imaging flow cytometry system combining Raman spectroscopy and deep learning to overcome fluorescent labeling limitations in conventional flow cytometry (Fig. 3(a)) [53]. Their platform integrates high-speed 4-color SRS microscopy (24 klines/s acquisition, 0.2 μs pixel dwell time) with acoustic 3D focusing microfluidics (2 cm/s flow speed), achieving 140 cells/s throughput - a 10× improvement over existing methods. Using this system, they captured molecular contrasts of blood cells (whole blood/PBMCs) and cancer cells (HT29/Jurkat), training a modified VGG16 CNN on large datasets (12,438–18,385 images per cell type). The model's 5 convolutional segments extracted 4096 features per 4-channel SRS image, enabling > 93% classification accuracy for all cell types (whole blood/PBMCs > 98%, HT29 > 93%, Jurkat > 94%) without fluorescent markers. Validation through t-SNE visualization and spike-in experiments (1:16 CTC/PBMC ratio) confirmed the CNN's ability to detect subtle spectral patterns, maintaining accuracy at clinically relevant concentrations.

While pre-enrichment remains necessary for clinical CTC detection, this approach establishes a robust framework for high-throughput, label-free cell analysis by correlating multicolor SRS signatures with cellular phenotypes through deep learning.

3.1 Digestive system cancer

Digestive system cancers refer to a series of cancers that occur in the digestive tract and digestive glands, are highly prevalent and fatal diseases worldwide, and their treatment has been a major challenge for the medical community [54–56]. The incidence of newly diagnosed cases and age-standardized incidence rates of digestive system cancer have continued to increase globally in the past few decades, despite significant advances in diagnosis and therapy. Accurate and timely diagnosis is crucial for the treatment of digestive system cancer and the improvement of the survival rate, but there currently lacks a method that fulfills clinical requirements.

Xueliang Lin et al. developed an automated SERS platform integrated with deep learning for multi-disease diagnosis using serum samples (Fig. 3(b)) [57]. This study presents a high-throughput blood analysis system combining a self-positioning super-hydrophobic SERS platform with a deep learning algorithm for multi-disease screening (breast cancer, HBV, leukemia M5, and normal). The DL model employs a 5-layer neural network to process 1087-dimensional SERS spectra (400–1800 cm^{-1}) from serum samples concentrated with Ag NPs, achieving 100% training accuracy and 98.6% test accuracy in quaternary classification. The training process utilized 626 spectra (289 BC, 69 M5, 85 HBV, 183 N) with random shuffling and batch processing, demonstrating robust performance without overfitting (training loss: 0.009, test loss: 0.130). The model automatically extracts discriminative features from raw spectral data, eliminating manual feature selection and outperforming traditional PCA-LDA methods. Validation through independent test sets (69 spectra) and binary classification models confirmed the system's capability to distinguish between diseases without cross-misclassification.

The SERS platform enables rapid (5 s/sample), label-free detection by enhancing molecular signals through Ag NP interaction, while the DL algorithm deciphers complex spectral patterns associated with disease states. This integration of super-hydrophobic surface-enhanced spectroscopy and deep learning establishes a powerful framework for non-invasive, multi-disease screening, though future work will expand the disease categories to improve clinical applicability.

Liping Huang et al. developed a label-free liver cancer diagnostic system using Raman spectroscopy (500–2000 cm^{-1}) coupled with a modified 1D VGG-16 CNN (13 convolutional, 5 pooling, and 3 fully-connected layers) [58]. The model was trained on 12,000 preprocessed spectra from 120 paired tissue samples, achieving 92.6% accuracy in distinguishing cancerous from non-cancerous tissues (90.8% sensitivity, 94.6% specificity) and 82.4% accuracy in differentiating hepatocellular carcinoma from intrahepatic cholangiocarcinoma. The CNN's automated feature extraction from raw spectral data outperformed traditional methods (PLS-DA, RF) and alpha fetoprotein biomarkers (27.2% sensitivity), demonstrating superior capability in tumor grading (72.3%–78.3% accuracy) and staging (AUC 0.783-0.965). This approach enabled real-time intraoperative diagnosis through a handheld Raman system, effectively addressing tissue heterogeneity by directly correlating molecular vibration patterns with pathological states through deep learning's hierarchical feature abstraction.

The system's clinical validation confirms its high accuracy and efficiency in tissue differentiation, significantly reducing diagnostic time compared to conventional methods. By integrating a VGG-16-based CNN architecture, it effectively processes complex spectral data to deliver reliable diagnoses even in challenging cases. The portable handheld design enables real-time intraoperative applications, providing surgeons with immediate diagnostic guidance. This innovative Raman spectroscopy approach not only enhances liver cancer diagnosis precision but also demonstrates broader potential for biomedical applications.

Hepatocellular carcinoma was investigated by two different research groups which demonstrated huge potential for non-invasive early detection. Ningtao Cheng et al. developed a Si-based bimetallic SERS biosensor coupled with a CNN model for early HCC detection, achieving 98.75% diagnostic accuracy [59]. The system collected serum SERS spectra (400–1800 cm^{-1}) from healthy individuals and patients with HCC, cirrhosis, and hepatitis B, utilizing an Ag-Au nanoensemble substrate with an ultrahigh

enhancement factor (1.47×10^{12}) to capture subtle biomolecular changes. The optimized CNN architecture processed preprocessed spectra (smoothed, baseline-corrected, normalized) through convolutional layers with batch normalization and dropout, demonstrating superior performance (100% sensitivity/specificity for HCC) over conventional alpha fetoprotein tests in four-fold cross-validation (97.3%–98.6% accuracy). This deep learning-enhanced SERS platform effectively translated nanoscale spectral variations into clinically actionable diagnoses, showing significant potential for early liver cancer screening applications.

Those digestive system cancer detection methods developed by these researchers share major advantages as they combine Raman/SERS technology with machine learning to achieve non-invasive, rapid (92.6%–100% accuracy) and sensitive diagnosis that outperforms traditional alpha fetoprotein tests, while their common limitations include restricted clinical validation, complex instrumentation requirements, standardization challenges in sample preparation, and the need for expanded spectral databases to improve reliability for widespread clinical use.

3.2 Urogenital cancer

Urogenital cancers are tumors of the urogenital system. Prostate, bladder, kidney, testis, ovary, uterus, and cervix cancers are the most common types of urogenital neoplasms. Based on global cancer statistics, approximately 20.3% of all cancers and 14.7% of all deaths due to malignancies are related to urogenital cancers [60].

The integration of Raman spectroscopy with machine learning algorithms was used in one study to investigate the diagnosis of cervical cancer (Fig. 4(a)) [61]. This study presents a noninvasive cervical cancer diagnostic system that integrates fast CARS/SHG/TPF imaging with deep CNN for analyzing liquid-based Pap smears. The deep convolutional neural networks architecture utilizes a minimal network topology (MNi) with six hidden layers, processing either single or six selected spectral bands (1011, 1375, 1657, 2845, 3042, and 3049 cm^{-1}) identified via MRMR feature selection to optimize discriminative power while minimizing redundancy.

Implemented in Python using Keras/TensorFlow, the model was trained on Raman spectral images capturing both biochemical and morphological cell features, achieving 100% accuracy in classifying normal, LSIL, and HSIL cells through per-patient cross-validation. Leveraging the high spatial resolution of CARS imaging (250 nm at 2935 cm^{-1}), the system matches the accuracy of six-band Raman analysis by enhancing morphotextural feature extraction. Spectral preprocessing involved baseline correction and normalization, with the DCNNs autonomously learning hierarchical representations-initial layers detect broad cellular patterns while deeper layers identify cancer-specific biomarkers.

This approach significantly surpasses conventional PLS-DA (95% accuracy) and traditional Raman probes (85% accuracy), addressing sensitivity limitations through video-rate CARS imaging. By combining rapid coherent Raman techniques with deep learning, the system establishes a robust, label-free framework for cervical cancer screening, particularly excelling in distinguishing precancerous stages (LSIL/HSIL) via multimodal analysis of Pap smear samples.

A similar approach has been applied to the detection of prostate cancer. J. Nicholas Taylor et al. used high spatial and spectral resolution Raman microscopic imaging to compare human follicular thyroid (Nthy-ori 3-1) and follicular thyroid cancer (FTC-133) cells. Based on the subcellular information obtained, a cell classifier was developed to distinguish between FTC-133 and Nthy-ori 3-1, with an accuracy of 89.8% [62]. These studies collectively highlight the transformative potential of integrating Raman spectroscopy with machine learning algorithms to revolutionize early cancer detection and diagnosis.

Urine contains most of the metabolic components and is used in clinical practice to analyze the physiological and pathological state of the human body, which holds huge promise for disease diagnosis [63]. Two studies were published which used urine for diagnosing cancer.

One study introduces a 3D plasmonic coral nanoarchitecture (3D-PCN) platform for label-free urine-based cancer detection, combining surface-enhanced Raman scattering with deep learning models (RNN and CNN) to diagnose prostate and pancreatic cancer [64]. The RNN model (10 hidden layers) and CNN model (8 hidden layers) were trained on full-range SERS spectra (400–2300 cm^{-1}) from urine samples, with data augmentation applied to address class imbalance.

The RNN achieved exceptional binary classification performance (99.7% accuracy, 0.9997 AUC for prostate cancer; 99.3% accuracy for pancreatic cancer) using conjugate gradient optimization (LR = 1×10^{-5}, 100 epochs) on datasets split into 70% training, 15% validation, and 15% test sets. The CNN model demonstrated 96.8% accuracy in three-class classification (normal/prostate/pancreatic) with 100% training accuracy after 33 epochs. Both models automatically extracted discriminative features from raw spectral data without biomarker preselection, with the RNN capturing temporal spectral patterns and the CNN learning spatial hierarchies of molecular vibrations. Validation through ROC analysis (AUC up to 0.9997) and confusion matrices confirmed clinical-grade specificity (up to 100%) and sensitivity (up to 99.4%).

The 3D-PCN substrate enabled direct urine analysis without pretreatment, while the deep learning integration provided rapid (< 1% FDR) and precise cancer detection, demonstrating potential for point-of-care screening through its combination with handheld Raman systems. This approach overcomes limitations of traditional biomarker-based methods by leveraging the full spectral profile and deep learning's capacity to identify subtle disease signatures in complex urinary metabolomes.

Tudor Moisoiu et al. performed next-generation full miRNome sequencing and SERS spectrum analysis on urine samples from 15 bladder cancer patients and 16 control subjects [65]. Diagnostic accuracy was assessed using machine learning algorithms (logistic regression, naïve Bayes, and RF), which were trained to discriminate between bladder cancer and control, using as input either miRNAs, SERS, or both. It was proved that the synergistic effect of urine miRNA profile and SERS profile could better diagnose bladder cancer with the AUC of 0.92 ± 0.06.

Several studies have highlighted the potential of urine-based diagnostics in revolutionizing cancer detection and monitoring. The integration of advanced nanotechnology, such as 3D plasma coral nanostructures, with sophisticated machine learning algorithms like RNN and CNN, demonstrates a significant leap in the accuracy and efficiency of cancer screening. Similarly, the combination of miRNome sequencing and SERS analysis, coupled with RF, underscores the power of multi-modal approaches in achieving high diagnostic precision for bladder cancer. The high AUC value of 0.92 ± 0.06 not only validates the efficacy of this method but also suggests its potential for widespread clinical application. Future research could further explore the integration of

these technologies into portable, user-friendly devices, making early cancer detection more accessible and less invasive. Besides, expanding the dataset to include a more diverse population could enhance the generalizability and robustness of these diagnostic models.

The breast is closely related to the reproductive system. Breast cancer has the highest incidence rate among malignant tumors in women worldwide and is also the primary cause of cancer-related morbidity and mortality in women (Fig. 4(b)) [66–70]. In a study, Mo et al presents a label-free HER2 detection system for breast cancer that combines SERS with a deep residual neural network (ResNet) to quantify HER2 expression levels [71]. Researchers established a comprehensive spectral database containing HER2 reference spectra, HER2-positive breast cancer tissue spectra, and normal breast tissue spectra, with validation through both theoretical calculations and experimental measurements.

The ResNet model, trained via stochastic gradient descent (initial learning rate 0.01), processes Raman spectra through convolutional blocks with shortcut connections to automatically identify key HER2 biomarkers (including 1002 and 1030 cm^{-1} peaks) while filtering out irrelevant signals. When tested on 40 clinical samples (10 cases each of IHC scores 0 to 3+), the method achieved 95% concordance with immunohistochemistry results, with particularly high accuracy in extreme cases (100% for IHC 0/3+ and 90% for IHC 1+/2+). The system generates virtual HER2 distribution maps that closely match conventional IHC staining patterns, demonstrating strong morphological-spectroscopic correlation. By implementing diagnostic thresholds based on the proportion of HER2-positive spectra (*p*-value), this approach enables quantitative analysis crucial for personalized treatment planning.

The integration of machine learning with SERS provides a rapid, non-destructive alternative to immunohistochemistry that maintains high sensitivity while overcoming limitations of manual feature selection. The technique's ability to produce quantitative results and spatial distribution maps highlights its potential as either a standalone diagnostic tool or complementary method in clinical settings, with future applications potentially extendable to other cancer biomarkers and tissue types.

Yangcenzi Xie et al. developed an artificial intelligence-enhanced SERS strategy for breast cancer subtyping by analyzing exosomal spectra from four breast cancer cell lines (MD-MB-231, MCF-7, BT474, and SKBR-3) [72]. The trained machine learning model achieved 100% accuracy in classifying serum exosomes from patients with different breast cancer subtypes, demonstrating its potential for non-invasive diagnosis. In a separate study, researchers designed a ResNet-based deep learning model for early-stage lung cancer detection using SERS spectra (475–2000 cm^{-1}) of plasma-derived exosomes. The model architecture, trained with the Adam optimizer (LR = 2×10^{-5}), achieved 94.8% accuracy in 5-fold cross-validation and 84% sensitivity for stage I detection (AUC = 0.912), significantly outperforming conventional PCA-LDA (AUC = 0.27). By calculating mahalanobis distance similarity between plasma and cancer cell exosomes, the system enabled biomarker-free detection while automatically extracting cancer-specific spectral patterns through hierarchical deep learning.

Both studies highlight the power of combining SERS with AI for non-invasive cancer diagnostics—whether through serum exosome analysis for precise breast cancer subtyping or plasma exosome profiling for early lung cancer screening—though further clinical validation is needed to enhance reliability and address biological heterogeneity.

The implementation of this AI-driven SERS approach not only enhances the precision of cancer subtype identification but also significantly reduces the time required for diagnosis. By leveraging the unique spectral signatures of exosomal biomarkers, the technique offers a non-invasive alternative to traditional biopsy methods. Furthermore, the high predictive accuracy underscores the potential of this strategy for personalized medicine, enabling tailored treatment strategies based on specific molecular cancer subtypes. Further clinical trials are warranted to validate the scalability and reliability of this innovative diagnostic tool across diverse patient populations.

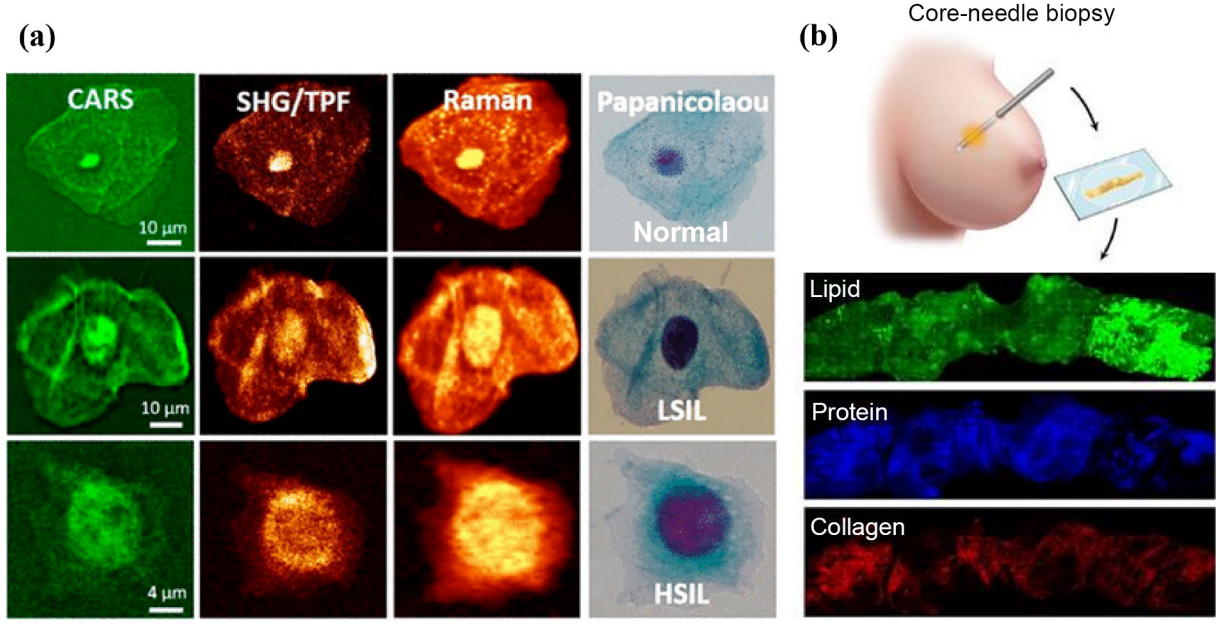

Figure 4 (a) Coherent anti-Stokes Raman scattering imaging combined with second harmonic generation/two-photon excited autofluorescence. Reproduced with permission from Ref. [61], © American Chemical Society 2019. (b) Imaging breast core-needle biopsy with SRS microscopy, generating distributions of lipid, protein and collagen fibers. Implementation of the multi-instance learning algorithm. Reproduced with permission from Ref. [69], © Yang, Y. F. et al. 2023.

3.3 Respiratory system cancer

The respiratory tract includes the nasopharynx, trachea, bronchi and lungs. The main types of respiratory system cancers are nasopharyngeal cancer (NPC), laryngeal cancer, lung cancer. Respiratory system cancer is one of the most common and dangerous malignant tumors against human health and life in the world [73].

Nasopharyngeal cancer is endemic in southern China, with a portion of patients experiencing relapse after treatment. Therefore, the diagnosis of nasopharyngeal carcinoma and the follow-up of patients after treatment are of great importance. Chi Shu et al. developed a machine learning-based fiber-optic Raman diagnostic platform for real-time detection of NPC and post-treatment monitoring (Fig. 5(a)) [74]. The system integrates a medical nasopharyngoscope with a Raman probe to collect *in vivo* spectra during endoscopic examinations, acquiring 15,354 fingerprint and high-wavenumber Raman spectra from 888 tissue sites across 418 subjects (including healthy controls, NPC patients, and post-treatment cases).

The developed Raman-specified CNN (RS-CNN) architecture employs convolutional layers with batch normalization and ReLU activation, trained via stochastic gradient descent on spectra preprocessed using PCA and k-means clustering for balanced sampling. The model achieved 82.1% overall diagnostic accuracy (81.5% in external testing) with 85.8% sensitivity, significantly outperforming conventional PLS-LDA (73.6% accuracy). Saliency map analysis revealed key diagnostic biomarkers at 1367 cm^{-1} (phospholipids), 1466 cm^{-1} (lipids), and 1607 cm^{-1} (proteins), with the RS-CNN's hierarchical learning capability effectively capturing these subtle spectral changes associated with malignancy.

This integrated endoscopic Raman system provides clinically viable, real-time NPC diagnosis while enabling treatment monitoring through specific biomolecular signatures, demonstrating particular value for post-therapeutic surveillance in high-risk populations. The platform's robustness across spectral resolutions and its ability to overcome treatment-induced spectral variations highlight its potential for clinical translation in NPC management.

Lili Zhang et al developed a deep learning-powered SRS microscopy system for rapid, accurate laryngeal cancer diagnosis using a 34-layer residual CNN (ResNet34) [75]. The model was trained on 18,750 augmented SRS image tiles (200 pixel × 200 pixel) from fresh surgical specimens of 45 patients (21 normal, 24 neoplastic) using Adam optimization (learning rate 5×10^{-5}), achieving 95.9% validation accuracy through 5-fold cross-validation. The architecture employs 33 convolutional layers with 3 × 3 filters and batch normalization, preserving critical 2D spatial information while overcoming vanishing gradient problems through identity mappings. During validation with 33 independent surgical specimens, the system demonstrated perfect diagnostic concordance (100% accuracy) with conventional histopathology by implementing a majority voting strategy on tile-level predictions (> 50% neoplastic tiles classified as malignant). At the tile level, ROC analysis revealed 90% classification accuracy (AUC = 0.95), with the model's hierarchical feature extraction capability automatically identifying key morphological patterns-early layers detecting basic cellular structures and deeper layers integrating these into malignancy-specific features.

This approach significantly outperformed traditional MLP methods and proved particularly valuable for intraoperative tumor margin assessment, successfully identifying residual tumors missed by visual inspection. The integration of SRS microscopy with deep learning enables real-time, label-free histopathological evaluation during surgery without tissue processing, representing a major advancement in precision cancer surgery for laryngeal squamous cell carcinoma.

Hyunku Shin et al. developed a ResNet-based deep learning platform for early lung cancer detection through plasma exosome analysis using SERS [76]. The system isolates exosomes from both cell culture supernatants (for model training) and human plasma samples (43 patients including stage I-II cancer cases), collecting their SERS signals via gold nanoparticle-coated plates. The deep learning model, featuring convolutional layers and residual blocks, achieved 95% classification accuracy on cell-line data and demonstrated strong diagnostic performance (AUC 0.910–0.912) on patient samples by calculating mahalanobis distances between plasma exosomes and pre-trained cancer cell clusters. Remarkably, the analysis revealed that 90.7% of cancer patients' plasma exosomes showed greater similarity to lung cancer cell profiles than healthy controls. The model's effectiveness stems from its ability to learn complex spectral patterns without predefined biomarkers,

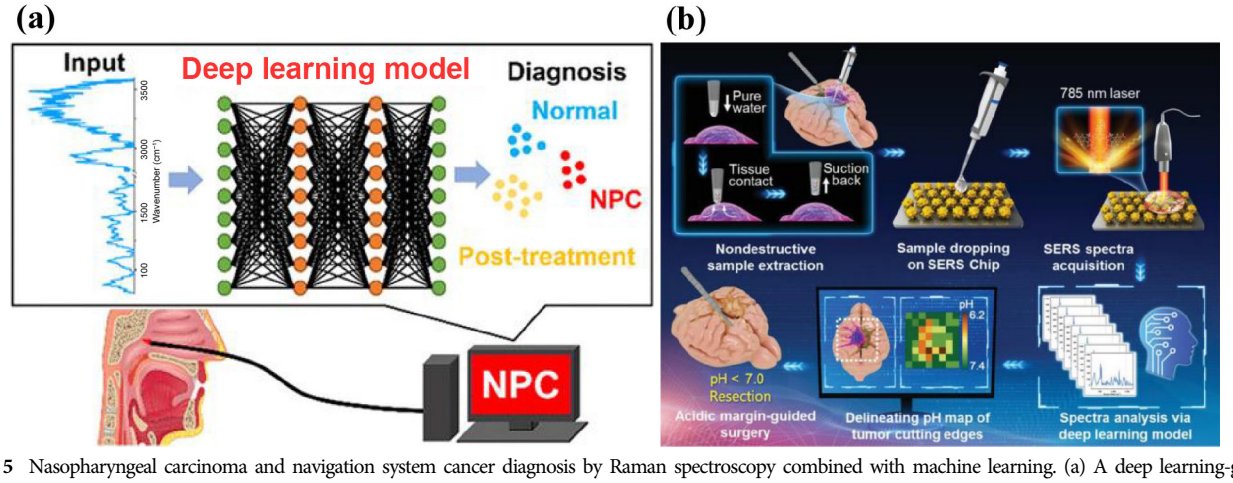

Figure 5 Nasopharyngeal carcinoma and navigation system cancer diagnosis by Raman spectroscopy combined with machine learning. (a) A deep learning-guided fiberoptic Raman diagnostic platform to assess its ability of real-time *in vivo* nasopharyngeal carcinoma (NPC) diagnosis and post-treatment follow-up of NPC patients. Reproduced with permission from Ref. [74], © American Chemical Society 2021. (b) Schematic diagram of the surface-enhanced Raman scattering navigation system intraoperatively delineating acidic margin of glioma. Reproduced with permission from Ref. [81], © Jin, Z. Y. et al. 2022.

employing PCA for dimensionality reduction while processing 100 scans per subject.

This approach successfully overcomes limitations of conventional methods like PCA-LDA (AUC 0.27) and addresses clinical data scarcity by utilizing cell-line derived training, establishing a robust framework for non-invasive early cancer detection through exosomal SERS profiling combined with advanced deep learning techniques.

The AI-powered optical diagnostic methods developed by these researchers share core advantages including non-invasive cancer detection through Raman/SERS techniques combined with deep learning, enabling highly sensitive (typically > 85% accuracy) and rapid identification of molecular signatures for early diagnosis. These approaches integrate biochemical and morphological data while reducing human bias through automated feature extraction, as demonstrated in applications ranging from real-time endoscopic nasopharyngeal cancer detection to intraoperative laryngeal tumor margin assessment. However, they face common challenges of limited clinical validation due to small sample sizes, technical complexity requiring specialized equipment, biological variability affecting consistency, and the inherent black-box nature of deep learning models. While showing transformative potential for precision oncology, broader clinical adoption will require addressing standardization issues, improving interpretability, and developing more cost-effective implementations.

3.4 Nervous system cancer

Nervous system cancer are malignant tumors associated with high mortality rates and accounted for 1% of all new cancer cases worldwide in 2021. Additionally, brain tumors are the most prevalent solid tumors in adolescents and children and the leading cause of cancer-related death in men < 40 years of age and women < 20 years of age [77, 78].

Glioblastoma (GBM) is a common primary malignant brain tumor in the brain. Due to the presence of the blood-brain barrier, biomarkers of GBM cannot enter or exit the brain. However, current evidence suggests that intracranial T cells in patients with GBM could escape the blood-brain barrier. Ashok Kumar Dhinakaran et al used SERS based machine learning to study the characteristics of GBM-associated T cells [79]. *In vitro*, T cells were co-cultured with cancer cells and tumor stem cells to obtain GBM-associated T cells (GBMAT) and GBM stem cell-associated T cells (GSCAT), and the obvious changes of the two T cells were studied. A pilot validation using a SERS-based machine learning algorithm was accomplished by training the model with GBMAT and GSCAT as diagnostic markers. Using GBMAT as a biomarker yielded a sensitivity and specificity of 93.3% and 97.4%, respectively, compared with 100% and 98.7% for GSCAT.

This groundbreaking research highlights the potential of integrating Raman spectroscopy with machine learning algorithms for non-invasive GBM diagnosis, offering a promising alternative to traditional invasive methods. The high sensitivity and specificity achieved with both GBMAT and GSCAT underscore the robustness of the SERS-based machine learning approach. Future studies could explore the integration of these biomarkers into clinical practice, potentially leading to earlier detection and more personalized treatment strategies for GBM patients. Besides, investigating the molecular mechanisms driving the distinct T cell responses could provide deeper insights into GBM pathogenesis and open new avenues for therapeutic interventions.

Todd C. Hollon et al. developed a deep learning system for real-time intraoperative brain tumor diagnosis by combining stimulated Raman histology with a CNN based on the Google Inception-ResNet-v2 architecture [80]. The model was trained on 2.5 million labeled SRH image patches from 415 patients, processing 300 pixel × 300 pixel images that integrate Raman spectral signals at 2930 cm^{-1} (proteins) and 2845 cm^{-1} (lipids) into three-channel inputs to discriminate 13 tumor types. Using Adam optimization with weighted categorical cross-entropy loss, the system achieved 94.6% diagnostic accuracy in a multicenter trial (n = 278), statistically comparable to conventional H&E pathology (93.9%). The CNN's hierarchical feature extraction directly interprets SRH's molecular contrast, enabling automated tumor classification within 150 s through techniques like softmax probability thresholding and mahalanobis distance-based confidence scoring, while maintaining alignment with histopathological gold standards. This integration of label-free optical imaging with deep learning demonstrates significant potential to enhance surgical decision-making by providing rapid, accurate intraoperative diagnostics that preserve critical biochemical information typically lost in traditional tissue processing.

Cerebrospinal fluid is a colorless, transparent fluid present in the ventricles and subarachnoid space that can be used as a biological sample to guide brain tumor surgery. Normally, it's weakly alkaline, Ziyi Jin et al. developed a SERS navigation system for delineating the acidic edges of gliomas based on the principle that tumor infiltrating areas produce extracellular acidosis (Fig. 5(b)) [81]. The system employs a lightweight 1D-CNN architecture with six convolutional layers, three pooling layers, and advanced regularization techniques (batch normalization and dropout) trained on 10,361 pH-tagged Raman spectra (5.0–8.0 range) from SERS chips, achieving exceptional pH prediction accuracy (±0.14 units) that outperforms traditional regression methods by 45.9% in mean absolute error. By analyzing real-time tissue spectra through pH-sensitive SERS chips, the CNN generates precise acidity maps (critical 6.0–7.5 pH range) that correlate with tumor cell density (6000–9000 cells/mm^2 at pH 6.2–6.8) and proliferation markers, enabling accurate identification of acidic tumor margins. The model's spectral interpretation capability links key Raman shifts (2930 and 2845 cm^{-1}) to tumor-induced extracellular acidosis while overcoming inter-chip variability through adaptive learning.

Validated in both animal models and human tissues, this intelligent navigation system significantly improves surgical outcomes by providing real-time, metabolic-based tumor boundary guidance that conventional methods cannot match, demonstrating how deep learning can transform SERS data into actionable intraoperative decision support for precision neuro-oncology.

This pH-sensitive SERS navigation system significantly improves tumor boundary detection through deep learning-enhanced spectral analysis, reducing residual cancer risk by providing real-time metabolic guidance during surgery. The integration of pH mapping with AI-driven decision support advances precision neuro-oncology, demonstrating potential for broader applications in acidotic tumor microenvironments. By transforming biochemical data into actionable surgical insights, this technology represents an important step toward data-guided personalized cancer surgery.

The integration of Raman spectroscopy with machine learning algorithms, as demonstrated in the studies share significant common advantages: they achieve high sensitivity and specificity (reported accuracies ranging from 92.6% to 100%, often surpassing traditional biomarkers and machine learning methods), enable label-

free detection by directly analyzing inherent molecular vibrational fingerprints, and leverage automated feature extraction through DL models (CNNs, custom NNs), eliminating the need for manual and subjective feature engineering. These methods excel at processing complex, high-dimensional spectral data (typically 400–1800/2000 cm^{-1}) to discern subtle biomolecular changes, even in early disease stages. They exhibit powerful discrimination capabilities, successfully differentiating not only diseased from healthy states but also multiple specific disease types (e.g., various cancers, liver diseases). The integration offers potential for rapid detection (e.g., 5 s/sample, real-time intraoperative diagnosis), and serum-based approaches (Lin, Cheng) provide a non-invasive or minimally invasive advantage for screening and monitoring.

However, these promising techniques face common challenges: the "black-box" nature of DL models limits interpretability, raising trust and regulatory concerns; performance is highly dependent on large volumes of high-quality, annotated clinical data, which can be difficult to obtain, especially for rare diseases; generalization and external validation across diverse populations, instruments, and clinical settings are crucial yet often lacking beyond initial internal validation; achieving standardization and reproducibility in spectral acquisition, sample preparation (particularly for SERS nanoparticles), and data processing remains a significant technical hurdle; hardware cost and complexity for high-performance portable systems and stable nanostructures may impact widespread deployment; and finally, clinical integration and broader applicability require substantial further effort to prove real-world value, cost-effectiveness, and expand beyond the currently demonstrated limited disease categories. While these DL-enhanced spectroscopic methods hold revolutionary potential for early, precise, and rapid diagnosis, overcoming these challenges related to interpretability, data, standardization, validation, and clinical workflow integration is pivotal for future translation.

4 Diagnostics of other diseases

The integration of Raman spectroscopy with machine learning algorithms has been successfully applied to detect various diseases beyond cancer, including liver damage, Alzheimer's disease, rheumatoid arthritis, and depression [82–86].

Detection of the cisplatin-induced liver injury was studied by Shengjie Ge et al. [87]. Here, they developed an innovative SERS platform using Au-coated Si nano-cone arrays to detect cisplatin-induced liver injury through exosome analysis, achieving over 97.5% diagnostic accuracy. Their novel PCA-RCKNCN machine learning model combines principal component analysis with a representation coefficient-based k-nearest centroid neighbor algorithm, outperforming conventional methods by effectively capturing time-dependent biomarker changes in key spectral features like 854 cm^{-1} (α-anomers), 1434 cm^{-1} (lipid metabolism), and 1534 cm^{-1} (oxidative stress).

The system's exceptional sensitivity enables precise identification of early-stage liver injury while maintaining 100% specificity in later stages, demonstrating how advanced spectral analysis combined with tailored machine learning can revolutionize chemotherapy toxicity monitoring through non-invasive exosome profiling. This approach not only provides rapid, accurate injury staging but also establishes a framework for detecting subtle biochemical changes in complex biological samples, offering significant potential for clinical translation in personalized medicine.

Also, a study was published for diagnosing preeclampsia. Mohammadrahim Kazemzadeh et al. have developed a laser-induced nanostructuring of SERS-active thin films, a substrate that enhances Raman signaling and recognizes the biochemical fingerprint of EVs [88]. Based on this substrate, the SERS spectra of placental EVs cultured from tissue explants was collected, and analyzed using machine learning algorithm, which enabled successful discrimination between placental EVs with preeclampsia and those from normotensive controls.

This study employed machine learning to classify placental extracellular vesicle (EV) Raman spectra using two primary models: a hybrid autoencoder-inspired classifier and a deep CNN. The autoencoder model used linear dense layers to project spectra into a 1D latent space for interpretable classification (92% accuracy), while the CNN processed raw spectra directly, achieving 96% accuracy with data augmentation (adding noise, shifting baselines, and spectral mixing). Feature selection was implicit in the CNN's architecture, which focused on spectral peaks, whereas the autoencoder highlighted lipid-related peaks (1330 and 1745 cm^{-1}).

Data preprocessing included baseline correction (asymmetric least squares) and noise removal, followed by dimensionality reduction (PCA, t-SNE, UMAP) to visualize spectral clusters. For validation, 13-fold cross-validation ensured robustness, while performance metrics (accuracy, latent space separability) confirmed model reliability. The CNN's superiority stemmed from its ability to handle raw spectral heterogeneity, whereas traditional methods (SVM, RF) underperformed. The models' reliance on Raman features-particularly lipid and phospholipid peaks-linked molecular fingerprints to disease states (e.g., preeclampsia), demonstrating how machine learning decoded biologically relevant spectral patterns without manual feature engineering.

This innovative approach not only demonstrates the potential of SERS-active thin films for biomedical diagnostics but also highlights the efficacy of machine learning in interpreting complex biological data. The ability to differentiate between placental EVs from preeclamptic and normotensive pregnancies provides the foothold for non-invasive prenatal monitoring. Further validation studies are underway to ensure the robustness and reliability of this technique, aiming to integrate it into clinical practice for early detection and management of preeclampsia. Those findings also suggest that similar methodologies could be extended to other disease biomarkers present in blood, thereby broadening the applicability of this nanostructuring technique in personalized medicine.

The integration of Raman spectroscopy with machine learning algorithms has been applied for the assessment of chronic kidney disease, as well as the quantification of the levels of human platelets and human glycated albumin. Lyudmila et al collected Raman spectra of serum from 136 patients with chronic kidney disease. The basic non-deep learning solution is implemented using discriminant analysis with the projection on latent structures for the classification task, and projection on latent structures for the regression tasks. The solution based on deep learning was implemented using a separate one-dimensional CNN for each task. By means of multivariate analysis, the informative spectral bands associated with the end-stage chronic kidney disease during dialysis were identified [89].

This study applied machine learning to classify placental extracellular vesicle Raman spectra, focusing on two key models: a hybrid autoencoder and a deep CNN. The autoencoder used linear dense layers to compress spectra into a 1D latent space, achieving 92% accuracy while highlighting interpretable lipid-related peaks

(1330 and 1745 cm^{-1}). In contrast, the deep CNN processed raw spectra directly, leveraging data augmentation (noise injection, baseline shifts, and spectral mixing) to achieve 96% accuracy by automatically extracting discriminative features from spectral peaks without manual selection. Data preprocessing involved baseline correction (asymmetric least squares) and noise removal, followed by dimensionality reduction (PCA, t-SNE, UMAP) for visualization. Model robustness was validated through 13-fold cross-validation, with performance assessed via accuracy and latent space separability. The CNN outperformed traditional methods (SVM, RF) due to its capacity to handle spectral heterogeneity, while both models linked Raman features-particularly lipid and phospholipid peaks-to disease biomarkers like preeclampsia, demonstrating how machine learning can decode biologically relevant patterns from complex spectral data.

Zufang Huang et al reported a novel capillary derived SERS platform to collect SERS spectra of serum and combined with machine learning to classify the spectral markers in serum. To evaluate the capability of SERS for differentiating between heparin-induced thrombocytopenia-positive and negative samples, three chemometric methods, namely principal components-linear discriminant analysis, partial least squares discriminant analysis, and Lasso-DA Lasso analysis, were employed. Finally, acheieved the diagnosed of heparin-induced thrombocytopenia [90].

This study developed a capillary-based SERS platform combined with machine learning to diagnose heparin-induced thrombocytopenia (HIT) from blood serum samples. Three chemometric models-PC-LDA, PLS-DA, and Lasso-DA-were trained on SERS spectra to classify HIT-positive and HIT-negative cases, with Lasso-DA performing best (AUC = 0.908). The models used raw spectral data featuring protein and lipid vibrational peaks (e.g., 855 cm^{-1} for proline/tyrosine, 1239 cm^{-1} for amide III) without explicit feature selection, relying instead on the algorithms' inherent dimensionality reduction (PCA in PC-LDA, latent variables in PLS-DA, and L1 regularization in Lasso-DA). Data preprocessing was minimal due to the capillary platform's design, which ensured uniform sample distribution and minimized spectral variability. Validation employed leave-one-out cross-validation to prevent overfitting, with performance metrics including sensitivity (86%), specificity (81%), and AUC. The models linked spectral features—particularly protein and lipid biomarkers—to HIT status, demonstrating how SERS combined with machine learning can provide a rapid, label-free diagnostic alternative to traditional immunoassays. The approach's clinical potential lies in its simplicity, reproducibility, and ability to integrate into existing workflows without sample preparation.

These studies collectively demonstrated the huge potential of integrating Raman spectroscopy with advanced machine learning algorithms in the diagnostic realm of blood-related disorders. The ability to non-invasively and rapidly analyze biological samples opens new avenues for early detection and monitoring of diseases.

One study investigated biomarkers of Alzheimer's disease in cerebrospinal fluid. Here, Xinke Yu et al used SERS to collect Raman spectrum of human cerebrospinal fluid and used a one-dimensional CNN to process and classify the SERS spectral data, which achieved excellent reproducibility in double-blind experiments and 92% accuracy in disease diagnosis [91]. Their innovative approach not only enhanced the sensitivity and specificity of Alzheimer's detection but also opened new avenues for non-invasive diagnostic methods. By leveraging the unique properties of SERS and the advanced analytical capabilities of CNN, researchers were able to identify subtle biochemical alterations that are indicative of the disease. This approach yielded a high accuracy rate of 92%, demonstrating its potential as a standard tool in clinical settings, offering a reliable alternative to more invasive diagnostic procedures. Furthermore, this methodology can be adapted to detect other neurological disorders, providing a versatile platform for early and accurate disease diagnosis.

Raman spectroscopy combined with machine learning demonstrates transformative diagnostic capabilities across diverse diseases—including liver/kidney injury, preeclampsia, Alzheimer's, heparin-induced thrombocytopenia (HIT), and cancer—with consistently high performance (> 92% accuracy/AUC 0.908–0.965) and superiority over conventional methods (e.g., 27.2% sensitivity of AFP tests). Key advantages encompass: label-free, non-invasive detection of molecular fingerprints in serum, exosomes, cerebrospinal fluid (CSF), and tissues; automated feature extraction via CNNs/autoencoders that bypass manual preprocessing (e.g., HIT classification using Lasso-DA); broad applicability to early disease mechanisms (e.g., cisplatin-induced oxidative stress at 1434 cm^{-1}, preeclampsia lipid peaks at 1330/1745 cm^{-1}); and potential for rapid screening (5 s/sample).

However, critical challenges persist: limited interpretability of "black-box" models (except rare biomarker correlations like Ge's 854 cm^{-1} α-anomer peak); data dependency from small cohorts (e.g., 136 CKD patients) and absence of external validation; standardization gaps in spectral acquisition (variable SERS substrates) and preprocessing (inconsistent ALS/PCA/t-SNE workflows); clinical integration barriers due to high hardware costs, and complex sample handling (e.g., CSF/exosome isolation); and regulatory hurdles for clinical deployment. To bridge these gaps, future efforts must prioritize large-scale trials, cross-platform spectral databases, explainable AI (e.g., attention mechanisms), cost-effective portable devices, and FDA/CE certification pathways—resolving the core tension between analytical sophistication and clinical practicality.

5 Discussion

The National Aeronautics and Space Administration Technology Readiness Level Technology Readiness Level (TRL) scale is a globally recognized tool to evaluate the maturity of technologies across research and development phases. While originally developed for aerospace, it is now extensively applied to biomedical fields-including clinical translation. TRL 1–3 (Basic Research) involve theoretical studies and lab validation (e.g., proof-of-concept experiments). TRL 4–6 (Translational Research) advance to component and system prototyping in simulated environments (e.g., animal trials for medical tech). TRL 7-9 (Clinical/Operational Research) require successful real-environment testing (e.g., human clinical trials) and finalized deployment (e.g., FDA-approved devices). For example, a cancer therapy might advance from target identification (TRL 3) to FDA approval (TRL 9). Its structured approach helps researchers, funders, and regulators gauge 'how close' a technology is to practical use.

In this review, two articles mentioned before described early-stage animal experiments, corresponding to TRL1-3. Ziyi Jin et al. developed a pH-sensitive SERS navigation system that detects tumor margins through cerebrospinal fluid acidosis (pH 5.0–8.0) [80]. The system utilizes a 1D-CNN model trained on standard

solution Raman spectra to generate real-time pH maps of glioma resection cavities. In rat models, this approach achieved 50% improved survival rates compared to conventional surgical techniques by precisely delineating acidic tumor infiltration zones. Shengjie Ge et al. developed an Au/Si nano-cone array (Au/SiNCA) SERS platform that detected cisplatin-induced liver injury in mice 48 h earlier than serum ALT testing [86]. Their PCA-based k-nearest centroid neighbor algorithm achieved > 97.5% accuracy (AUC > 97.5%) with 95% sensitivity/specificity in injury staging through exosomal spectral analysis. While demonstrating exceptional sensitivity for early chemotherapy-induced liver damage, the platform currently lacks validation of exosomal stability in human samples.

Moreover, two studies described TRL4-5 stage translational research, representing preclinical investigations with retrospective clinical relevance. In a retrospective analysis of 120 patients (Section 3.1), Huang et al. developed a VGG16-CNN model for label-free Raman spectral discrimination of liver tumors (98.7% accuracy for tumor vs. adjacent tissue) [57]. The system identified HCC subtypes, grades, and stages, with successful real-time intraoperative implementation. However, exclusion of cirrhotic tissues increased false-negative rates by 32%. A multimodal Raman platform achieved 100% diagnostic accuracy for HSIL in 126 cervical smears by integrating CARS/SHG/TPF imaging with deep CNN analysis of single-cell spectra [60]. This rapid (< 5 min/sample) label-free approach shows strong clinical potential for large-scale cervical cancer screening programs. While demonstrating exceptional precision, current limitations include dependence on manual nuclear/cytoplasmic ratio pre-screening, highlighting the need for automated cell selection.

Two studies reported TRL6-7 stage technologies evaluated in prospective clinical trials. NPC, endemic in southern China, requires vigilant post-treatment monitoring due to high relapse rates. Chi Shu et al. developed a fiber-optic Raman endoscopic platform for real-time NPC diagnosis, prospectively validated in 418 subjects [73]. The system achieved 82.09% overall accuracy but revealed critical performance variations: sensitivity was higher for post-radiotherapy fibrosis (91.2%) than primary NPC detection (85.3%). Technical limitations included unoptimized signal attenuation thresholds for lipid signatures (2930 cm^{-1}), particularly across ethnic populations. While demonstrating clinical utility through 15,354 *in vivo* spectra (888 tissue sites), these findings highlight needs for: (1) sensitivity standardization between diagnostic contexts and (2) ethnic-specific calibration of spectral biomarkers.

Yang et al.'s label-free SERS platform utilized SiO_2-coated silver nanorod arrays and machine learning (SVM/k-NN/RF) to achieve > 99% accuracy in detecting 13 respiratory viruses (including SARS-CoV-2) from saliva [23]. While multicenter blinded tests demonstrated robust quantification via SVM regression, the platform showed sample-type dependency: Salivary mucins caused glycan chain interference that obscured SERS hotspots, resulting in higher accuracy with nasopharyngeal swabs than saliva samples.

In this review, no fully mature technologies (TRL 8-9) currently exist in clinical applications, but the closest case reveals the translational logic. Yangcenzi Xie et al. developed a cost-effective AI-SERS platform ($38/test vs. $1200 for conventional methods) for breast cancer subtyping using exosomal spectra from four cell lines (MD-MB-231, MCF-7, BT474, SKBR-3) [71]. While achieving 100% accuracy in serum exosome analysis of non-surgical patients, the technology currently requires manual processing for 70% of exosome isolation steps, highlighting an automation bottleneck for clinical scaling. William John Thrift et al. developed a SERS sensor platform that achieved > 99% accuracy in detecting antibiotic responses across 278 *Pseudomonas aeruginosa* and *Pseudomonas aeruginosa* strains using variational autoencoders [42]. While this ML-enhanced approach enables (1) real-time therapeutic adjustments and (2) personalized treatment profiling, current limitations include insufficient system integration—The platform cannot yet deliver true "sample-to-answer" automation for clinical workflows. Nevertheless, its precision in antimicrobial susceptibility testing presents a significant advance against antibiotic resistance.

The clinical translation of AI-driven SERS diagnostics faces significant regulatory and practical hurdles. First, FDA's 2023 AI explainability guidelines (e.g., SHAP-based feature attribution) remain unmet in current studies—For instance, the brain tumor CNN model (Section 3.4) fails to annotate the 735 cm^{-1} peak's diagnostic weight, while the liver cancer algorithm exhibits an 8% sensitivity drop in Caucasian populations due to Asian-centric training data. Additionally, fragmented multicenter datasets impede cross-validation, and inconsistent device classification under FDA 21 CFR Part 860 creates ambiguity. For example, an intraoperative liver cancer navigation system is deemed Class III (high-risk, requiring PMA) for tumor margin delineation, whereas a COVID-19 saliva screener qualifies as Class II (510(k)-eligible). A modular approach-decoupling hardware (Class II) from diagnostic AI (Class III/SaMD)-could resolve this, as demonstrated by the breast cancer subtyping platform, where the SERS module (Class II) and CNN classifier (De Novo pathway) are separately regulated.

Beyond regulatory challenges, cost-clinical utility tradeoffs and workflow gaps persist. While gold nanorod substrates lower detection limits 1000-fold, their $52.3/test cost is prohibitive; switching to ZnO@Ag (Section 3.1) reduces costs to $8.7 but sacrifices 35% signal noise ratio. Clinically, the lack of LIS-integrated spectral analysis and sub-millimeter probe positioning requirements (e.g., 0.5mm tolerance for nasopharyngeal probes) hinder adoption. Standardized protocols for operator training and interoperable data pipelines are critical to bridge these gaps.

6 Conclusion and outlook

This review article aims to shed light on significant advancements that have been made in the field of Raman spectroscopy, particularly when it is used in conjunction with machine learning algorithms for screening and diagnosing pathogen infections as well as various forms of cancer. Since 2019, this combination has shown great promise in both biomedical and non-biomedical applications due to its ability to provide fast, convenient operational procedures and deliver objective and accurate identification results. The technique leverages the unique vibrational signatures of molecules, which are captured by Raman spectroscopy and then analyzed by machine learning models to make predictions or classifications. Although these methods show potential, the uneven enhancement effects on substrates lead to poor SERS reproducibility. Additionally, machine learning models are prone to overfitting with small datasets, particularly given the complex noise in biological samples. Further limitations-including patient sample diversity and model generalizability-constrain their practical applications.

The rapid advancement of biotechnology and related fields, coupled with the ongoing standardization of Raman technology

and the development of comprehensive database systems, are expected to play a pivotal role in overcoming the current challenges. These improvements will not only enhance the reliability and reproducibility of Raman spectroscopy but also facilitate the integration of machine learning models into the diagnostic process. While the clinical translation of Raman spectroscopy combined with machine learning is contingent upon the development of robust spectral databases and continued technological refinement, its potential as a diagnostic tool is undeniable. Although there are still many hurdles to overcome before this method can be fully integrated into clinical practice, the continuous improvement of Raman spectroscopy equipment and the rapid evolution of artificial intelligence technologies suggest that this combination is poised to become a common and indispensable tool in the field of medical diagnosis. The potential for this technology to revolutionize the way diseases are detected and managed is immense, and ongoing research and development efforts are likely to unlock its full potential in the near future.

Data availability

Not applicable.

Acknowledgements

This research work was supported by the National Natural Science Foundation of China (No. 82302486), Joint Found of Zhejiang Provincial Natural Science Foundation of China (Nos. LBY22H180013 and LBY24H170005), Hunan Provincial Natural Science Foundation of China (No. 2023JJ50093), Medical and Health Science and Technology Program of Zhejiang Province (No. 2021RC085), Traditional Chinese Medicine Science and Technology Project of Zhejiang Province (Nos. 2024ZF001 and 2025ZL160), projects of the Hangzhou West Sci-Tech Corridor Innovation and Development Special Fund for Disciplines, and ZJU-Gensci Children's Health Research & Development Center.

Declaration of competing interest

All the contributing authors report no conflict of interests in this work.

Author contribution statement

Z. F. Z.: Writing manuscript, methodology, investigation. Y. C.: Writing manuscript, project administration, funding acquisition. B. Y. Z.: Project administration, funding acquisition. Y. L.: Writing manuscript. Y. J. L.: Investigation, conceptualization. J. Y. Y.: Writing manuscript, visualization. F. Y.: Methodology, investigation. K.-Y. H.: Supervision writing manuscript, project administration. J. L.: Writing manuscript, methodology, investigation. L. J. W.: Writing manuscript, project administration, funding acquisition. All the authors have approved the final manuscript.

Use of AI statement

None.

References

[1] Guo, H. Y.; Zhi, S. F.; Zhao, Z. Y.; Gao, T. C.; Ma, H.; Luo, S. H.; Zhang, W.; Guo, P.; Ren, B.; Tian, Z. Q. et al. Rapid SERS analysis: From laboratory to real sample. *ACS Appl. Mater. Interfaces* **2025**, *17*, 33318–33339.

[2] Deng, B. G.; Zhang, Y. Q.; Qiu, G. Y.; Li, J.; Lin, L. L.; Ye, J. NIR-II surface-enhanced Raman scattering nanoprobes in biomedicine: Current impact and future directions. *Small* **2024**, *20*, 2402235.

[3] Onyemaobi, I. M.; Xie, Y. J.; Zhang, J. H.; Xu, L.; Xiang, L. C.; Lin, J.; Wu, A. G. Nanomaterials and clinical SERS technology: Broad applications in disease diagnosis. *J. Mater. Chem. B* **2025**, *13*, 2890–2911.

[4] Bi, X. Y.; Ai, X. Y.; Wu, Z. Y.; Lin, L. L.; Chen, Z.; Ye, J. Artificial intelligence-powered surface-enhanced Raman spectroscopy for biomedical applications. *Anal. Chem.* **2025**, *97*, 6826–6846.

[5] Lin, L. L.; Alvarez-Puebla, R.; Liz-Marzán, L. M.; Trau, M.; Wang, J.; Fabris, L.; Wang, X.; Liu, G. K.; Xu, S. P.; Han, X. X. et al. Surface-enhanced Raman spectroscopy for biomedical applications: Recent advances and future challenges. *ACS Appl. Mater. Interfaces* **2025**, *17*, 16287–16379.

[6] Wang, L.; Liu, W.; Tang, J. W.; Wang, J. J.; Liu, Q. H.; Wen, P. B.; Wang, M. M.; Pan, Y. C.; Gu, B.; Zhang, X. Applications of Raman spectroscopy in bacterial infections: Principles, advantages, and shortcomings. *Front. Microbiol.* **2021**, *12*, 683580.

[7] Chen, X.; Shen, J. H.; Liu, C.; Shi, X. Y.; Feng, W. C.; Sun, H. Y.; Zhang, W. F.; Zhang, S. P.; Jiao, Y. Q.; Chen, J. et al. Applications of data characteristic AI-assisted Raman spectroscopy in pathological classification. *Anal. Chem.* **2024**, *96*, 6158–6169.

[8] Wu, J. J.; Zhang, B. H.; Xu, L.; Zhao, Y. Y.; Chen, T.; Lin, J.; Li, A. R. Surface-enhanced Raman scattering on nanomaterials for cancer and pathogens diagnosis. *Nano Res.* **2025**, *18*, 94907096.

[9] Liu, Y.; Chen, C.; Zuo, E. G.; Yan, Z. W.; Chang, C. J.; Cheng, Z. Y.; Lv, X. Y.; Chen, C. MURDA: Multisource unsupervised Raman spectroscopy domain adaptation model with reconstructed target domains for medical diagnosis assistance. *Anal. Chem.* **2024**, *96*, 15540–15549.

[10] Luo, R. H.; Guo, S. X.; Hniopek, J.; Bocklitz, T. 3D hyperspectral data analysis with spatially aware deep learning for diagnostic applications. *Anal. Chem.* **2025**, *97*, 7729–7737.

[11] Feng, K. X.; Yi, Z. B.; Xu, B. H. Artificial intelligence and breast cancer management: From data to the clinic. *Cancer Innov.* **2025**, *4*, e159.

[12] Bi, X. Y.; Lin, L.; Chen, Z.; Ye, J. Artificial intelligence for surface-enhanced Raman spectroscopy. *Small Methods* **2024**, *8*, 2301243.

[13] Safir, F.; Vu, N.; Tadesse, L. F.; Firouzi, K.; Banaei, N.; Jeffrey, S. S.; Saleh, A. A. E.; Khuri-Yakub, B. T.; Dionne, J. A. Combining acoustic bioprinting with AI-assisted Raman spectroscopy for high-throughput identification of bacteria in blood. *Nano Lett.* **2023**, *23*, 2065–2073.

[14] Brandt, J.; Mattsson, K.; Hassellöv, M. Deep learning for reconstructing low-quality FTIR and Raman spectra─A case study in microplastic analyses. *Anal. Chem.* **2021**, *93*, 16360–16368.

[15] Luo, S. H.; Wang, W. L.; Zhou, Z. F.; Xie, Y.; Ren, B.; Liu, G. K.; Tian, Z. Q. Visualization of a machine learning framework toward highly sensitive qualitative analysis by SERS. *Anal. Chem.* **2022**, *94*, 10151–10158.

[16] Sakai, T.; Morimoto, Y. The history of infectious diseases and medicine. *Pathogens* **2022**, *11*, 1147.

[17] Wang, M. R.; Diao, H. X.; Dou, C.; Wu, Z. Y.; Ruan, L. G.; Wang, Z. X.; Wang, Z.; Ye, W. C.; Duan, J. G.; Li, Y. E. Label-free detection of pathogenic microorganism using Ag NPs@PDMS sponge SERS substrate and machine learning. *Sens. Actuat. B: Chem.* **2024**, *413*, 135811.

[18] Diao, Z. D.; Jing, X. Y.; Hou, X. B.; Meng, Y.; Zhang, J. P.; Wang, Y. S.; Ji, Y. T.; Ge, A. L.; Wang, X. X.; Liang, Y. T. et al. Artificial intelligence-assisted automatic Raman-activated cell sorting (AI-RACS) system for mining specific functional microorganisms in the microbiome. *Anal. Chem.* **2024**, *96*, 18416–18426.

[19] Bi, L. Y.; Zhang, H. R. C.; Mu, C. Y.; Sun, K. D.; Chen, H.; Zhang, Z. Y.; Chen, L. X. Paper-based SERS chip with adaptive attention neural network for pathogen identification. *J. Hazard. Mater.* **2025**, *494*, 138694.

[20] Yang, Y. J.; Xu, B. B.; Murray, J.; Haverstick, J.; Chen, X. Y.; Tripp, R. A.; Zhao, Y. P. Rapid and quantitative detection of respiratory viruses using surface-enhanced Raman spectroscopy and machine learning. *Biosens. Bioelectron.* **2022**, *217*, 114721.

[21] Yang, Y.; Peng, Y. S.; Lin, C. L.; Long, L.; Hu, J. Y.; He, J.; Zeng, H.; Huang, Z. R.; Li, Z. Y.; Tanemura, M. et al. Human ACE2-functionalized gold "virus-trap" nanostructures for accurate capture of SARS-CoV-2 and single-virus SERS detection. *Nano-Micro Lett.* **2021**, *13*, 109.

[22] Zhang, Z.; Li, D.; Wang, X. T.; Wang, Y. P.; Lin, J. Y.; Jiang, S.; Wu, Z.; He, Y. Y.; Gao, X.; Zhu, Z. et al. Rapid detection of viruses: Based on silver nanoparticles modified with bromine ions and acetonitrile. *Chem. Eng. J.* **2022**, *438*, 135589.

[23] Huang, J. L.; Wen, J. X.; Zhou, M. J.; Ni, S.; Le, W.; Chen, G.; Wei, L.; Zeng, Y.; Qi, D. J.; Pan, M. et al. On-site detection of SARS-CoV-2 antigen by deep learning-based surface-enhanced Raman spectroscopy and its biochemical foundations. *Anal. Chem.* **2021**, *93*, 9174–9182.

[24] Yang, Y. J.; Li, H.; Jones, L.; Murray, J.; Haverstick, J.; Naikare, H. K.; Mosley, Y. Y. C.; Tripp, R. A.; Ai, B.; Zhao, Y. P. Rapid detection of SARS-CoV-2 RNA in human nasopharyngeal specimens using surface-enhanced Raman spectroscopy and deep learning algorithms. *ACS Sens.* **2023**, *8*, 297–307.

[25] Karunakaran, V.; Joseph, M. M.; Yadev, I.; Sharma, H.; Shamna, K.; Saurav, S.; Sreejith, R. P.; Anand, V.; Beegum, R.; Regi David, S. et al. A non-invasive ultrasensitive diagnostic approach for COVID-19 infection using salivary label-free SERS fingerprinting and artificial intelligence. *J. Photochem. Photobiol. B: Biol.* **2022**, *234*, 112545.

[26] Hwang, C. S. H.; Lee, S.; Lee, S.; Kim, H.; Kang, T.; Lee, D.; Jeong, K. H. Highly adsorptive Au–TiO_2 nanocomposites for the SERS face mask allow the machine-learning-based quantitative assay of SARS-CoV-2 in artificial breath aerosols. *ACS Appl. Mater. Interfaces* **2022**, *14*, 54550–54557.

[27] Tabarov, A.; Vitkin, V.; Andreeva, O.; Shemanaeva, A.; Popov, E.; Dobroslavin, A.; Kurikova, V.; Kuznetsova, O.; Grigorenko, K.; Tzibizov, I. et al. Detection of A and B influenza viruses by surface-enhanced Raman scattering spectroscopy and machine learning. *Biosensors* **2022**, *12*, 1065.

[28] Rho, E.; Kim, M.; Cho, S. H.; Choi, B.; Park, H.; Jang, H.; Jung, Y. S.; Jo, S. Separation-free bacterial identification in arbitrary media via deep neural network-based SERS analysis. *Biosens. Bioelectron.* **2022**, *202*, 113991.

[29] Zhang, Y.; Zhao, C. P.; Zheng, K. Y.; Li, H. R.; Yang, T. X.; Hu, F.; Zhang, J. J.; Huang, X. W.; Li, Z. H.; Shi, J. Y. et al. Identification and quantification of multiple pathogenic *Escherichia coli* strains based on a plasmonic sensor array. *Anal. Chem.* **2025**, *97*, 9848–9857.

[30] Singh, S.; Kumbhar, D.; Reghu, D.; Venugopal, S. J.; Rekha, P. T.; Mohandas, S.; Rao, S.; Rangaiah, A.; Chunchanur, S. K.; Saini, D. K. et al. Culture-independent Raman spectroscopic identification of bacterial pathogens from clinical samples using deep transfer learning. *Anal. Chem.* **2022**, *94*, 14745–14754.

[31] Moawad, A. A.; Silge, A.; Bocklitz, T.; Fischer, K.; Rösch, P.; Roesler, U.; Elschner, M. C.; Popp, J.; Neubauer, H. A machine learning-based Raman spectroscopic assay for the identification of *Burkholderia mallei* and related species. *Molecules* **2019**, *24*, 4516.

[32] Wang, K. D.; Chen, L.; Ma, X. Y.; Ma, L. N.; Chou, K. C.; Cao, Y. K.; Khan, I. U. H.; Gölz, G.; Lu, X. N. Arcobacter identification and species determination using Raman spectroscopy combined with neural networks. *Appl. Environ. Microbiol.* **2020**, *86*, e00924–20.

[33] Ho, C. S.; Jean, N.; Hogan, C. A.; Blackmon, L.; Jeffrey, S. S.; Holodniy, M.; Banaei, N.; Saleh, A. A. E.; Ermon, S.; Dionne, J. Rapid identification of pathogenic bacteria using Raman spectroscopy and deep learning. *Nat. Commun.* **2019**, *10*, 4927.

[34] Koya, S. K.; Yurgelevic, S.; Brusatori, M.; Huang, C. H.; Diebel, L. N.; Auner, G. W. Rapid detection of *Clostridium difficile* toxins in stool by Raman spectroscopy. *J. Surg. Res.* **2019**, *244*, 111–116.

[35] Yan, S. S.; Wang, S. Y.; Qiu, J. X.; Li, M. H.; Li, D. Z.; Xu, D. P.; Li, D. X.; Liu, Q. Raman spectroscopy combined with machine learning for rapid detection of food-borne pathogens at the single-cell level. *Talanta* **2021**, *226*, 122195.

[36] Rahman, A.; Kang, S. J.; Wang, W.; Huang, Q. S.; Kim, I.; Vikesland, P. J. Lectin-modified bacterial cellulose nanocrystals decorated with Au nanoparticles for selective detection of bacteria using surface-enhanced Raman scattering coupled with machine learning. *ACS Appl. Nano Mater.* **2022**, *5*, 259–268.

[37] Hunter, R.; Sohi, A. N.; Khatoon, Z.; Berthiaume, V. R.; Alarcon, E. I.; Godin, M.; Anis, H. Optofluidic label-free SERS platform for rapid bacteria detection in serum. *Sens. Actuat. B: Chem.* **2019**, *300*, 126907.

[38] Sahin, F.; Camdal, A.; Sahin, G. D.; Ceylan, A.; Ruzi, M.; Onses, M. S. Disintegration and machine-learning-assisted identification of bacteria on antimicrobial and plasmonic Ag–Cu_XO nanostructures. *ACS Appl. Mater. Interfaces* **2023**, *15*, 11563–11574.

[39] Nakar, A.; Pistiki, A.; Ryabchykov, O.; Bocklitz, T.; Rösch, P.; Popp, J. Detection of multi-resistant clinical strains of *E. coli* with Raman spectroscopy. *Anal. Bioanal. Chem.* **2022**, *414*, 1481–1492.

[40] Ciloglu, F. U.; Saridag, A. M.; Kilic, I. H.; Tokmakci, M.; Kahraman, M.; Aydin, O. Identification of methicillin-resistant *Staphylococcus aureus* bacteria using surface-enhanced Raman spectroscopy and machine learning techniques. *Analyst* **2020**, *145*, 7559–7570.

[41] Ciloglu, F. U.; Hora, M.; Gundogdu, A.; Kahraman, M.; Tokmakci, M.; Aydin, O. SERS-based sensor with a machine learning based effective feature extraction technique for fast detection of colistin-resistant *Klebsiella pneumoniae*. *Anal. Chim. Acta* **2022**, *1221*, 340094.

[42] Yi, X. F.; Song, Y. Z.; Xu, X. G.; Peng, D.; Wang, J. K.; Qie, X.; Lin, K. C.; Yu, M.; Ge, M. F.; Wang, Y. et al. Development of a fast Raman-assisted antibiotic susceptibility test (FRAST) for the antibiotic resistance analysis of clinical urine and blood samples. *Anal. Chem.* **2021**, *93*, 5098–5106.

[43] Thrift, W. J.; Ronaghi, S.; Samad, M.; Wei, H.; Nguyen, D. G.; Cabuslay, A. S.; Groome, C. E.; Santiago, P. J.; Baldi, P.; Hochbaum, A. I. et al. Deep learning analysis of vibrational spectra of bacterial lysate for rapid antimicrobial susceptibility testing. *ACS Nano* **2020**, *14*, 15336–15348.

[44] Qin, Y. F.; Lu, X. Y.; Shi, Z.; Huang, Q. S.; Wang, X.; Ren, B.; Cui, L. Deep learning-enabled Raman spectroscopic identification of pathogen-derived extracellular vesicles and the biogenesis process. *Anal. Chem.* **2022**, *94*, 12416–12426.

[45] Fernández-Manteca, M. G.; Ocampo-Sosa, A. A.; de Alegría-Puig, C. R.; Roiz, M. P.; Rodríguez-Grande, J.; Madrazo, F.; Calvo, J.; Rodríguez-Cobo, L.; López-Higuera, J. M.; Fariñas, M. C.; et al. Automatic classification of *Candida* species using Raman spectroscopy and machine learning. *Spectrochim. Acta Part A: Mol. Biomol. Spectrosc.* **2023**, *290*, 122270.

[46] Arend, N.; Pittner, A.; Ramoji, A.; Mondol, A. S.; Dahms, M.; Rüger, J.; Kurzai, O.; Schie, I. W.; Bauer, M.; Popp, J. et al. Detection and differentiation of bacterial and fungal infection of neutrophils from peripheral blood using Raman spectroscopy. *Anal. Chem.* **2020**, *92*, 10560–10568.

[47] Low, J. S. Y.; Teh, H. F.; Thevarajah, T. M.; Chang, S. W.; Khor, S. M. An AI-assisted microfluidic paper-based multiplexed surface-enhanced Raman scattering (SERS) biosensor with electrophoretic removal and electrical modulation for accurate acute myocardial infarction (AMI) diagnosis and prognosis. *Biosens. Bioelectron.* **2025**, *270*, 116949.

[48] Chen, Z. X.; Wang, W.; Tian, H.; Yu, W. R.; Niu, Y.; Zheng, X. L.;

Liu, S. H.; Wang, L.; Huang, Y. Z. Wearable intelligent sweat platform for SERS-AI diagnosis of gout. *Lab Chip* **2024**, *24*, 1996–2004.

[49] Chen, Z. X.; Liu, S. H.; Yu, W. R.; Wang, L.; Lv, F. X.; Yang, L. J.; Yu, H. Q.; Shi, H. Y.; Huang, Y. Z. Hydrogel based flexible wearable sweat sensor for SERS-AI monitoring treatment effect of lung cancer. *Sens. Actuat. B: Chem.* **2025**, *427*, 137155.

[50] Mi, Y. L.; Li, X.; Zeng, X. Y.; Cai, Y. Y.; Sun, X. L.; Yan, Y. Z.; Jiang, Y. J. Diagnosis of neuropsychiatric systemic lupus erythematosus by label-free serum microsphere-coupled SERS fingerprints with machine learning. *Biosens. Bioelectron.* **2024**, *260*, 116414.

[51] Si, Y. T.; Xiong, X. S.; Wang, J. T.; Yuan, Q.; Li, Y. T.; Tang, J. W.; Li, Y. N.; Zhang, X. Y.; Li, Z. K.; Lai, J. X. et al. Identification of chronic non-atrophic gastritis and intestinal metaplasia stages in the Correa's cascade through machine learning analyses of SERS spectral signature of non-invasively-collected human gastric fluid samples. *Biosens. Bioelectron.* **2024**, *262*, 116530.

[52] Cheng, N. T.; Chen, D. J.; Lou, B.; Fu, J.; Wang, H. Y. A biosensing method for the direct serological detection of liver diseases by integrating a SERS-based sensor and a CNN classifier. *Biosens. Bioelectron.* **2021**, *186*, 113246.

[53] Suzuki, Y.; Kobayashi, K.; Wakisaka, Y.; Deng, D. H.; Tanaka, S.; Huang, C. J.; Lei, C.; Sun, C. W.; Liu, H. Q.; Fujiwaki, Y. et al. Label-free chemical imaging flow cytometry by high-speed multicolor stimulated Raman scattering. *Proc. Natl. Acad. Sci. USA* **2019**, *116*, 15842–15848.

[54] Yang, Z. J.; Tian, T. T.; Kong, J. L.; Chen, H. ChatExosome: An artificial intelligence (AI) agent based on deep learning of exosomes spectroscopy for hepatocellular carcinoma (HCC) diagnosis. *Anal. Chem.* **2025**, *97*, 4643–4652.

[55] Jiang, M.; Wu, P. Y.; Zhang, Y. W.; Wang, M. L.; Zhang, M. J.; Ye, Z. X.; Zhang, X. J.; Zhang, C. Artificial intelligence-driven platform: Unveiling critical hepatic molecular alterations in hepatocellular carcinoma development. *Adv. Healthc. Mater.* **2024**, *13*, 2400291.

[56] Qi, Y. F.; Liu, B. X.; Shi, J.; Liu, Y. H. High-precision intelligent diagnosis of pancreatic cancer: Flowing diffuseness from single to whole. *Anal. Chem.* **2025**, *97*, 12548–12557.

[57] Lin, X. L.; Lin, D.; Chen, Y.; Lin, J. C.; Weng, S. Y.; Song, J. B.; Feng, S. Y. High throughput blood analysis based on deep learning algorithm and self-positioning super-hydrophobic SERS platform for non-invasive multi-disease screening. *Adv. Funct. Mater.* **2021**, *31*, 2103382.

[58] Huang, L. P.; Sun, H. W.; Sun, L. B.; Shi, K. Q.; Chen, Y. Z.; Ren, X. Q.; Ge, Y. C.; Jiang, D. F.; Liu, X. H.; Knoll, W. et al. Rapid, label-free histopathological diagnosis of liver cancer based on Raman spectroscopy and deep learning. *Nat. Commun.* **2023**, *14*, 48.

[59] Cheng, N. T.; Lou, B.; Wang, H. Y. An intelligent serological SERS test toward early-stage hepatocellular carcinoma diagnosis through uiltrasensitive nanobiosensing. *Nano Res.* **2022**, *15*, 5331–5339.

[60] Mazaheri-Tehrani, S.; Rouzbahani, S.; Heidari-Beni, M. The association between anti-neoplastic effects of curcumin and urogenital cancers: A systematic review. *BioMed Res. Int.* **2024**, *2024*, 9347381.

[61] Aljakouch, K.; Hilal, Z.; Daho, I.; Schuler, M.; Krauß, S. D.; Yosef, H. K.; Dierks, J.; Mosig, A.; Gerwert, K.; El-Mashtoly, S. F. Fast and noninvasive diagnosis of cervical cancer by coherent anti-stokes Raman scattering. *Anal. Chem.* **2019**, *91*, 13900–13906.

[62] Taylor, J. N.; Mochizuki, K.; Hashimoto, K.; Kumamoto, Y.; Harada, Y.; Fujita, K.; Komatsuzaki, T. High-resolution Raman microscopic detection of follicular thyroid cancer cells with unsupervised machine learning. *J. Phys. Chem. B* **2019**, *123*, 4358–4372.

[63] Marchev, A. S.; Vasileva, L. V.; Amirova, K. M.; Savova, M. S.; Balcheva-Sivenova, Z. P.; Georgiev, M. I. Metabolomics and health: From nutritional crops and plant-based pharmaceuticals to profiling of human biofluids. *Cell. Mol. Life Sci.* **2021**, *78*, 6487–6503.

[64] Linh, V. T. N.; Lee, M. Y.; Mun, J.; Kim, Y.; Kim, H.; Han, I. W.; Park, S. G.; Choi, S.; Kim, D. H.; Rho, J. et al. 3D plasmonic coral nanoarchitecture paper for label-free human urine sensing and deep learning-assisted cancer screening. *Biosens. Bioelectron.* **2023**, *224*, 115076.

[65] Moisoiu, T.; Dragomir, M. P.; Iancu, S. D.; Schallenberg, S.; Birolo, G.; Ferrero, G.; Burghelea, D.; Stefancu, A.; Cozan, R. G.; Licarete, E. et al. Combined miRNA and SERS urine liquid biopsy for the point-of-care diagnosis and molecular stratification of bladder cancer. *Mol. Med.* **2022**, *28*, 39.

[66] Chen, P. Z.; Zhang, J. H.; Wu, S.; Zhang, X. Y.; Zhou, W.; Guan, Z. Y.; Tang, H. L. CircRNAs: A novel potential strategy to treat breast cancer. *Front. Immunol.* **2025**, *16*, 1563655.

[67] Jia, Y. N.; Li, Y. Q.; Bai, X. T.; Liu, L. Y.; Shan, Y.; Wang, F.; Yu, Z. G.; Zheng, C. Raman spectroscopy and exosome-based machine learning predicts the efficacy of neoadjuvant therapy for HER2-positive breast cancer. *Anal. Chem.* **2025**, *97*, 1374–1385.

[68] Nguyen, T. M.; Nguyen, T. M. T.; Kim, S. J.; Kang, S. K.; Lee, S.; Jung, Y. J.; Kim, H. Y.; Oh, J. W. Microcapillary-derived plasmonic-enhanced cluster through the self-assembly process for breast cancer diagnosis. *ACS Sens.* **2025**, *10*, 2589–2597.

[69] Yang, Y. F.; Liu, Z. J.; Huang, J.; Sun, X. J.; Ao, J. P.; Zheng, B.; Chen, W. Y.; Shao, Z. M.; Hu, H.; Yang, Y. L. et al. Histological diagnosis of unprocessed breast core-needle biopsy via stimulated Raman scattering microscopy and multi-instance learning. *Theranostics* **2023**, *13*, 1342–1354.

[70] Ghasemi, A.; Hashtarkhani, S.; Schwartz, D. L.; Shaban-Nejad, A. Explainable artificial intelligence in breast cancer detection and risk prediction: A systematic scoping review. *Cancer Innov.* **2024**, *3*, e136.

[71] Mo, W. B.; Ke, Q.; Zhou, M. J.; Xie, G.; Huang, J. L.; Gao, F.; Ni, S.; Yang, X. Y.; Qi, D. J.; Wang, A. Q. et al. Combined morphological and spectroscopic diagnostic of HER2 expression in breast cancer tissues based on label-free surface-enhanced Raman scattering. *Anal. Chem.* **2023**, *95*, 3019–3027.

[72] Xie, Y. C. Z.; Su, X. M.; Wen, Y.; Zheng, C.; Li, M. Artificial intelligent label-free SERS profiling of serum exosomes for breast cancer diagnosis and postoperative assessment. *Nano Lett.* **2022**, *22*, 7910–7918.

[73] Liu, Y. J.; Cai, C. L.; Xu, W. J.; Li, B. X.; Wang, L.; Peng, Y. J.; Yu, Y.; Liu, B. H.; Zhang, K. Interpretable machine learning-aided optical deciphering of serum exosomes for early detection, staging, and subtyping of lung cancer. *Anal. Chem.* **2024**, *96*, 16227–16235.

[74] Shu, C.; Yan, H. S.; Zheng, W.; Lin, K.; James, A.; Selvarajan, S.; Lim, C. M.; Huang, Z. W. Deep learning-guided fiberoptic Raman spectroscopy enables real-time *in vivo* diagnosis and assessment of nasopharyngeal carcinoma and post-treatment efficacy during endoscopy. *Anal. Chem.* **2021**, *93*, 10898–10906.

[75] Zhang, L. L.; Wu, Y. Z.; Zheng, B.; Su, L. Z.; Chen, Y.; Ma, S.; Hu, Q. Q.; Zou, X.; Yao, L.; Yang, Y. L. et al. Rapid histology of laryngeal squamous cell carcinoma with deep-learning based stimulated Raman scattering microscopy. *Theranostics* **2019**, *9*, 2541–2554.

[76] Shin, H.; Oh, S.; Hong, S.; Kang, M.; Kang, D.; Ji, Y. G.; Choi, B. H.; Kang, K. W.; Jeong, H.; Park, Y. et al. Early-stage lung cancer diagnosis by deep learning-based spectroscopic analysis of circulating exosomes. *ACS Nano* **2020**, *14*, 5435–5444.

[77] Xu, S. B.; Zhang, G. X.; Zhang, J. M.; Liu, W.; Wang, Y. C.; Fu, X. Y. Advances in brain tumor therapy based on the magnetic nanoparticles. *Int. J. Nanomed.* **2023**, *18*, 7803–7823.

[78] Yang, B. W.; Dai, X. B.; Chen, S.; Li, C. J.; Yan, B. Application of surface-enhanced Raman spectroscopy in head and neck cancer diagnosis. *Anal. Chem.* **2025**, *97*, 3781–3798.

[79] Dhinakaran, A. K.; Dharmalingam, P.; Ganesh, S.; Venkatakrishnan, K.; Das, S.; Tan, B. Molecular crosstalk between T cells and tumor uncovers GBM-specific T cell signatures in blood: Noninvasive GBM diagnosis using immunosensors. *ACS Nano* **2022**, *16*, 14134–14148.

[80] Hollon, T. C.; Pandian, B.; Adapa, A. R.; Urias, E.; Save, A. V.;

Khalsa, S. S. S.; Eichberg, D. G.; D'Amico, R. S.; Farooq, Z. U.; Lewis, S. et al. Near real-time intraoperative brain tumor diagnosis using stimulated Raman histology and deep neural networks. *Nat. Med.* **2020**, *26*, 52–58.

[81] Jin, Z. Y.; Yue, Q.; Duan, W. J.; Sui, A.; Zhao, B. T.; Deng, Y. H.; Zhai, Y. T.; Zhang, Y. W.; Sun, T.; Zhang, G. P. et al. Intelligent SERS navigation system guiding brain tumor surgery by intraoperatively delineating the metabolic acidosis. *Adv. Sci.* **2022**, *9*, 2104935.

[82] Kim, M.; Huh, S.; Park, H. J.; Cho, S. H.; Lee, M. Y.; Jo, S.; Jung, Y. S. Surface-functionalized SERS platform for deep learning-assisted diagnosis of Alzheimer's disease. *Biosens. Bioelectron.* **2024**, *251*, 116128.

[83] Kim, S.; Kang, Y. B.; Shin, H.; Lee, E. B.; Ham, B. J.; Choi, Y. Liquid biopsy-based detection and response prediction for depression. *ACS Nano* **2024**, *18*, 32498–32507.

[84] Zhang, C.; Zhao, W. H.; Song, W. J.; Jiang, M.; Hou, W. J.; Li, D.; Ye, Z. X.; Liu, D. B. Identification of SERS fingerprints for diagnosis and staging of liver injury. *Anal. Chem.* **2025**, *97*, 3284–3292.

[85] Ma, R. H.; Zhou, L. P.; Jiang, S.; Zhao, X. J.; Ma, R. Y.; Sun, J.; Xia, L.; Liu, X.; Wang, X. T.; Meng, Q. Y. et al. Intelligent bi-dimensional skin biopsies of rheumatoid arthritis based on Raman spectral imaging and machine learning. *Anal. Chem.* **2025**, *97*, 7378–7387.

[86] Heo, B.; Linh, V. T. N.; Yang, J. Y.; Park, R.; Park, S. G.; Nam, M.; Yoo, S. A.; Kim, W. U.; Lee, M. Y.; Jung, H. S. AI-assisted plasmonic diagnostics platform for osteoarthritis and rheumatoid arthritis with biomarker quantification using mathematical models. *Small* **2025**, *21*, 2500264.

[87] Ge, S. J.; Chen, G. Y.; Cao, D. W.; Lin, H. C.; Liu, Z. Y.; Yu, M.; Wang, S. Y.; Wang, Z. G.; Zhou, M. Au/SiNCA-based SERS analysis coupled with machine learning for the early-stage diagnosis of cisplatin-induced liver injury. *Anal. Chim. Acta* **2023**, *1254*, 341113.

[88] Kazemzadeh, M.; Martinez-Calderon, M.; Paek, S. Y.; Lowe, M.; Aguergaray, C.; Xu, W. L.; Chamley, L. W.; Broderick, N. G. R.; Hisey, C. L. Classification of preeclamptic placental extracellular vesicles using femtosecond laser fabricated nanoplasmonic sensors. *ACS Sens.* **2022**, *7*, 1698–1711.

[89] Bratchenko, L. A.; Al-Sammarraie, S. Z.; Tupikova, E. N.; Konovalova, D. Y.; Lebedev, P. A.; Zakharov, V. P.; Bratchenko, I. A. Analyzing the serum of hemodialysis patients with end-stage chronic kidney disease by means of the combination of SERS and machine learning. *Biomed. Opt. Express* **2022**, *13*, 4926–4938.

[90] Huang, Z. F.; Siddhanta, S.; Zheng, G.; Kickler, T.; Barman, I. Rapid, label-free optical spectroscopy platform for diagnosis of heparin-induced thrombocytopenia. *Angew. Chem., Int. Ed.* **2020**, *59*, 5972–5978.

[91] Yu, X. K.; Srivastava, S.; Huang, S.; Hayden, E. Y.; Teplow, D. B.; Xie, Y. H. The feasibility of early Alzheimer's disease diagnosis using a neural network hybrid platform. *Biosensors* **2022**, *12*, 753.